

**SYNTHESIS AND CHARACTERISATION OF COPPER
SELENIDE NANOPARTICLES VIA EMULSION TECHNIQUE**

By

CHONG WEI SOON

A project report submitted to the Department of Chemical Science

Faculty of Science,

Universiti Tunku Abdul Rahman,

In partial fulfillment of requirements for the degree of

Bachelor of Science (Hons) Chemistry

May 2011

ABSTRACT

Copper selenide (CuSe) nanoparticles had been successfully synthesised by using copper(II) chloride dihydrate ($\text{CuCl}_2 \cdot 2\text{H}_2\text{O}$) and sodium selenite (Na_2SeO_3) in ternary oil-in-water (o/w) emulsion system. The reducing agent, sodium borohydride (NaBH_4) used to reduce sodium selenite source in synthesising CuSe at room temperature. The sizes of the CuSe nanoparticles were determined by X-Ray diffractometer. Visible optical spectroscopy study was carried out to determine the band gap of the nanostructure CuSe and also to understand the quantum confinement of the CuSe. The crystallite size of synthesised CuSe samples are around 8.0447 – 20.2958 nm. The band gap energy was found in the range of 1.87 – 2.40 eV. Besides that, the samples were also examined with Photoluminescence (PL) Spectrophotometer and an emission peak was observed in the visible range at about 438 nm.

ABSTRAK

kuprum selenide (CuSe) nanopartikel telah berjaya disintesis dengan tindak balas antara kuprum klorida-dihidrat ($\text{CuCl}_2 \cdot 2\text{H}_2\text{O}$) dan natrium selenite (Na_2SeO_3) dalam sistem emulsi. Agen penurunan NaBH_4 (Natrium Borohidrida) telah digunakan untuk sintesis CuSe pada suhu bilik. Spektrometer pembelauan sinar-X (XRD) telah digunakan untuk menentukan band gap CuSe nanostruktur. Saiz kristal yang sampel CuSe disintesis adalah di antara 8.0447 – 20.2958 nm. Tenaga band gap yang ditemui adalah dalam lingkungan di antara 1.87 – 2.40 eV. Selain itu, Spektrometer Fotoluminasi juga telah digunakan untuk menganalisis sampel-sampel tersebut. Puncak spektrum untuk kesemua spektrum telah didapati pada panjang gelombang sekitar 438 nm.

ACKNOWLEDGEMENTS

I will begin my acknowledgement by sincerely thanking my supervisor, Dr. Saravanan Nagalingam for his guidance during the period of completing this project by providing numerous suggestions and valuable knowledge. His patience in guiding and continuous help was the main essence that keeps me working till the end. I would also like to express my gratitude to him for granting me freedom and positive attitude in completing this research.

Secondly, I would like to thank my fellow research team mates - Yong Siok San and Leong Kah Meng as well as laboratory assistant for their valuable comments and ideas on this work. Next, special thanks also go to Edwin kam, Bee Chong, Ar Qing, Mean Chuan and those who have helped me for being so supportive and keep me motivated along the way.

I would like to take this opportunity to thank my parents and siblings for giving me support constantly to overcome all the obstacles faced in completing this project and the degree of program.

APPROVAL SHEET

I certify that, this project entitled “SYNTHESIS AND CHARACTERISATION OF COPPER SELENIDE NANOPARTICLES VIA EMULSION TECHNIQUE” was prepared by CHONG WEI SOON and submitted in partial fulfillment of the requirements for the degree of Bachelor of Science (Hons) in chemistry at Universiti Tunku Abdul Rahman.

Approved by

Supervisor

Date: _____

(Dr. Saravanan Nagalingam)

Assistant Professor

**FACULTY OF SCIENCE
UNIVERSITI TUNKU ABDUL RAHMAN**

Date: _____

PERMISSION SHEET

It is hereby certified that CHONG WEI SOON (08ADB06252) has completed this report entitled “SYNTHESIS OF COPPER SELENIDE NANOPARTICLES USING EMULSION TECHNIQUE” under supervisor of ASSISTANT PROFERSSOR DR. SARAVANAN NAGALINGAM from the Department Chemical Science, Faculty of Science.

I hereby give permission to my supervisor to write and prepared manuscript of these research findings for publishing in any form, if I did not prepare it within six (6) months’ time from this date provided that my name is included as one of the authors for this article. Arrangement of the name depends on my supervisor.

DECLARATION

I hereby declare that this project report is based on my original work except for citations and quotations which have been duly acknowledged. I also declare that it has not been previously and concurrently submitted for any other degree or award at UTAR or other institutions.

CHONG WEI SOON

Date:

TABLE OF CONTENTS

	Page
ABSTRACT	ii
ABSTRAK	iii
ACKNOWLEDGEMENT	iv
APPROVAL SHEET	v
PERMISSION SHEET	vi
DECLARATION	vii
LIST OF TABLES	xi
LIST OF FIGURES	xii
LIST OF ABBREVIATION	xvi
CHAPTER	
1. INTRODUCTION	1
1.1. Nanotechnology	1
1.2. Nanometer	1
1.3. Nanomaterial	2
1.3.1. One-dimension Nanomaterials (1-D)	3
1.3.1.1 Thin Films, layers and surfaces	3
1.3.2 Two-dimensional Nanomaterials (2-D)	4
1.3.2.1 Carbon Nanotubes	4
1.3.2.2 Nanowires	6
1.3.3 Three-dimensional Nanomaterials (3-D)	6
1.3.3.1 Quantum dots	6
1.3.3.2 Nanoparticles	9
1.3.4 Effect of the Changes in Dimension	10
1.3.4.1 Changes to the system total energy	10
1.3.4.2 Changes to the system structure	11

1.4	Applications of Nanotechnology	11
1.4.1	Sunscreens and Cosmetics	12
1.4.2	Catalysts	12
1.4.3	Tougher and harder Cutting tools	13
1.4.4	Heterogeneous nanostructures & composites	13
1.4.5	Sensors	14
1.4.6	Therapeutic drugs	14
1.4.7	Drugs delivery	15
1.4.8	Optical electronics	15
1.4.9	Transistor	15
1.5	Fabrication methods	16
1.5.1	Top down approach	17
1.5.2	Bottom up approach	17
1.5.3	Template growth of nanomaterials	18
1.5.3.1	Differences of Microemulsion & emulsion system	18
1.6	CuSe and Its application	20
1.7	Objectives	21
2	LITERATURE REVIEW	22
2.1	Microemulsion and the Formation of Micelles Structure	22
2.2	Effect of CTAB on the formation of nanoparticle	25
2.3	Water/oil volume ratio effects on the formation of CuInSe ₂	27
2.4	Duration effects on the microstructures of CuInSe ₂ Powders	29
2.5	Effect of reaction temperature on the microstructures of CuInSe ₂ powders	32
2.6	Template free-solvothermally synthesised copper selenide (CuSe, Cu _{2-x} Se, b-Cu ₂ Se and Cu ₂ Se) hexagonal nanoplates from different precursors at low temperature	34
2.7	The effect of annealing on vacuum-evaporated copper selenide and indium telluride thin films	35
2.8	Physical, optical and electrical properties of copper selenide (CuSe) thin films deposited by solution growth technique at room temperature	37
2.9	Optical properties and electrical conductivity studies of copper selenide nanoparticle	39
2.10	Photon absorption in direct and indirect band gap Semiconductor	41

3	METHODOLOGY	42
3.1	Chemical used	42
3.2	Apparatus	42
3.3	Synthesis of Copper Selenide using Ternary Water-in-oil emulsion system	43
3.3.1	Effect of reducing Agent Concentration	43
3.3.2	Effect of stirring	46
3.3.3	Effect of autoclaved period	47
3.3.4	Centrifugation of samples	48
3.4	Characterisation	49
3.4.1	X-ray Diffraction (XRD)	50
3.4.2	Optical Properties	53
3.4.3	Photoluminescence (PL) Spectrophotometer	55
4	RESULTS AND DISCUSSION	57
4.1	X-Ray Diffractometer	57
4.2	UV/Vis spectrometer (optical properties)	70
4.3	Photoluminescence Spectrophotometer	79
5	CONCLUSION AND RECOMMENDATIONS	84
	BIBLIOGRAPHY	86
	APPENDICES	93

LIST OF TABLES

Table		page
1.1	Comparison of emulsion and microemulsion	19
2.1	The optical band gap was measured at room temperature for CuSe	41
3.1	Chemical used to synthesis Copper selenide (CuSe) nanoparticles	42
3.2	Preparation of sample at various concentrations of reducing agent (NaBH ₄)	44
3.3	Preparation of CuSe sample at different period (time of stirring)	46
3.4	Preparation of CuSe sample at various heated-treatment periods	47
4.1	XRD data for sample prepared at various reducing agent concentration	61
4.2	XRD data for sample prepared at various stirring period	63
4.3	XRD data for sample prepared at various heated-treatment period	65
4.4	Comparison of mean crystallite size for seven samples	67
4.5	Comparison of band gap energy values of samples prepared and literature band gap energy values	78
4.6	Summary of the emission peak and fluorescence intensity for all samples prepared in different parameters	79

LIST OF FIGURES

Figure		page
1.1	The comparison of size with different matters	2
1.2	Molecular structures of a single-walled carbon nanotube (SWNT) and of a multi-walled carbon nanotube (MWNT)	5
1.3	The band diagram for nano-sized crystals of semiconductor (quantum dots)	7
1.4	Colloidal quantum dots irradiated with a UV light. Different sized quantum dots emit different color light due to quantum confinement.	8
1.5	Nanoparticles in water suspension exhibit different colours depending on the size and shape	10
1.6	Schematic representation of the building up of Nanostructures	16
2.1	Structure of inverse micelle and normal micelle	23
2.2	Comparison between water in oil emulsion and oil in water Emulsion	24
2.3	XRD patterns of CuInSe ₂ powders prepared at 200 °C for 3 h with the W/O volume ratios of (a) 1:5, (b) 1:10, and (c) 1:15 in the microemulsion-mediated solvothermal process	28
2.4	XRD patterns of CuInSe ₂ powders prepared at 200 °C for (a) 30 min, (b) 1 h, (c) 3 h, and (d) 5 h with the W/O volume ratio of 1:15 in the microemulsion-mediated solvothermal process	30
2.5	TEM micrographs of CuInSe ₂ powders prepared at 200 °C for (a) 30 min, (b) 1 h, (c) 3 h, and (d) 5 h with the W/O volume ratio of 1:15 in the microemulsion-mediated solvothermal process	31

2.6	XRD patterns of CuInSe ₂ powders prepared at (a) 160 °C, (b) 180 °C, (c) 200 °C, and (d) 220 °C for 3 h with the W/O volume ratio of 1:15 in the microemulsion-mediated solvothermal process	33
2.7	TEM micrographs of CuInSe ₂ powders prepared at (a) 160 °C, (b) 180 °C, (c) 200 °C, and (d) 220 °C for 3 h with the W/O volume ratio of 1:15 in the microemulsion-mediated solvothermal process	33
2.8	X-ray diffractogram of as-deposited and 473 K annealed CuSe films	36
2.9	Plot of $(\alpha h\nu)^2$ vs. $h\nu$ for CuSe thin films	38
2.10	The relation between absorbance and wavelength for CuSe Prepared at T=160 °C, T=170 °C and T=200 °C dispersed in absolute ethanol	39
2.11	Relation between $(\alpha h\nu)^2$ and photon energy ($h\nu$) for CuSe prepared at T=160 °C, 170 °C and T=200 °C	40
2.12	<i>E-k</i> diagram illustrating a) Photon absorption in a direct band gap semiconductor b) Photon absorption in an indirect band gap semiconductor assisted by phonon absorption and c) Photon absorption in an indirect band gap semiconductor assisted by phonon emission.	41
3.1	Flowchart of synthesising CuSe at various concentration of reducing agent, NaBH ₄	45
3.2	Centrifugation instrument model Sigma Sartorius 2-1	48
3.3	Shimadzu X-ray Diffractometer (LabX XRD-6000)	50
3.4	Diagram for Bragg reflection from a set of crystal planes with a spacing of d	51
3.5	A schematic diagram of a powder diffractometer	52
3.6	Perkin Elmer Lambda 35 UV/Vis Spectrophotometer	53

3.7	Diagram of double beam UV/Vis spectrometer	54
3.8	Fluorescence Spectrophotometer, Pelkin Elmer Precisely LS 55	55
3.9	Energy level diagram of fluorescence occurrence	56
4.1	Formation of micelle system in synthesis of copper selenide nanoparticles	58
4.2	XRD pattern of samples prepared at various reducing agent concentration, $[\text{NaBH}_4]\text{M}$	60
4.3	XRD pattern of samples prepared at various periods (under stirring condition)	62
4.4	XRD pattern of samples prepared at various periods (under autoclave condition)	64
4.5	UV/Vis absorption spectrum of CuSe nanoparticles at different concentration of reducing agent S3020 = 2.0 M, S3025 = 2.5 M, S3030 = 3.0 M, respectively	70
4.6	UV/Vis absorption of CuSe nanoparticles prepared at different period (under stirring condition) S3020 = 1 hour, S30202 = 2 hours and S30203 = 3hours	71
4.7	UV/Vis absorption of CuSe nanoparticles prepared at different period (under autoclave condition) S3020 = 30 minutes, S6020 = 60 minutes, and S9020 = 90 minutes	72
4.8	Relation between $(\alpha h\nu)^2$ and photon energy $(h\nu)$ for CuSe nanoparticle prepared at various reducing agent, NaBH_4 S3020 = 2.0 M, S3025 = 2.5 M and S3030 = 3.0 M	75
4.9	Relation between $(\alpha h\nu)^2$ and photon energy $(h\nu)$ for CuSe nanoparticle prepared at various time of stirring S3020 = 1 h, S30202 = 2 h and S30203 = 3h	76
4.10	Relation between $(\alpha h\nu)^2$ and photon energy $(h\nu)$ for CuSe nanoparticle prepared at various time of stirring S3020 = 30 mins, S6020 = 60mins and S9020 = 90 mins	77

4.11	Photoluminescence spectrum of control set for the synthesis of copper selenide	80
4.12	PL spectra of all the CuSe samples prepared at different concentration of reducing agent used	80
4.13	PL spectra of all the CuSe samples prepared at different stirring period	81
4.14	PL spectra of all the CuSe samples prepared at different heated-treatment period	81

LIST OF ABBREVIATIONS/ SYMBOLS

$\text{CuCl}_2 \cdot 2\text{H}_2\text{O}$	Copper(II) chloride dihydrate
Na_2SeO_3	Sodium selenite
$\text{C}_{19}\text{H}_{42}\text{BrN}$	N-Cetyl-N,N,N-trimethylammonium Bromide
C_6H_{12}	Cyclohexane
NaBH_4	Sodium borohydride
$\text{C}_2\text{H}_5\text{OH}$	Absolute ethanol
CMC	Critical Micelle Concentration
o/w	oil in water
w/o	water in oil
XRD	X-Ray Diffractometer
UV-Vis	UV-visible
PL	Photoluminescence
Å	Angstrom (10^{-10}m)
α	Alpha
β	Beta
γ	Gamma
π	Pi
λ	Lambda
θ	Theta

°C	Degree in Celsius
eV	Electron Volt
g	Gram
m	Mili
M	Concentration in molL ⁻¹
mL	Mililiter
nm	Nanometer (10 ⁻⁹ m)
μm	Micrometer (10 ⁻⁶ m)
At%	Percentage of atom
E	Energy
<i>h</i>	Plank's constant (6.63 x 10 ⁻³⁴ Js)
<i>c</i>	Speed of light (3.0 x 10 ⁸ ms ⁻¹)
<i>v</i>	Velocity

CHAPTER 1

INTRODUCTION

1.1 Nanotechnology

Nanoscience is the study of phenomena and manipulation of material at the nanoscale; it is an extension of existing sciences into the nanoscale (Dutta and Gupta, 2008).

Nanotechnology refers to technological study and application involving nanoparticles. It is manipulating matter on an atomic and molecular scale and dealing with structures sized between 1 to 100 nanometers in at least one dimension, and involves developing materials or devices within that size. Nanotechnology may be able to create many new materials and devices with a vast range of applications, such as in medicine, electronics, biomaterials and energy production (Asiyanbola and Soboyejo, 2008). Nanoparticle has been applied loosely to include all particles less than 1 micrometer.

1.2 Nanometer

Nanometer is a unit of spatial measurement that is 10^{-9} meter. It is commonly used in nanotechnology, the building of extremely small machines. A

nanometer in size of substance can be seen by using powerful microscope like Atomic Force Microscope. Atoms and molecules and the smallest pieces of everything around us, are measured in nanometers (Monasi, 2008). The Figure 1.1 below shows the comparison of size of different items.

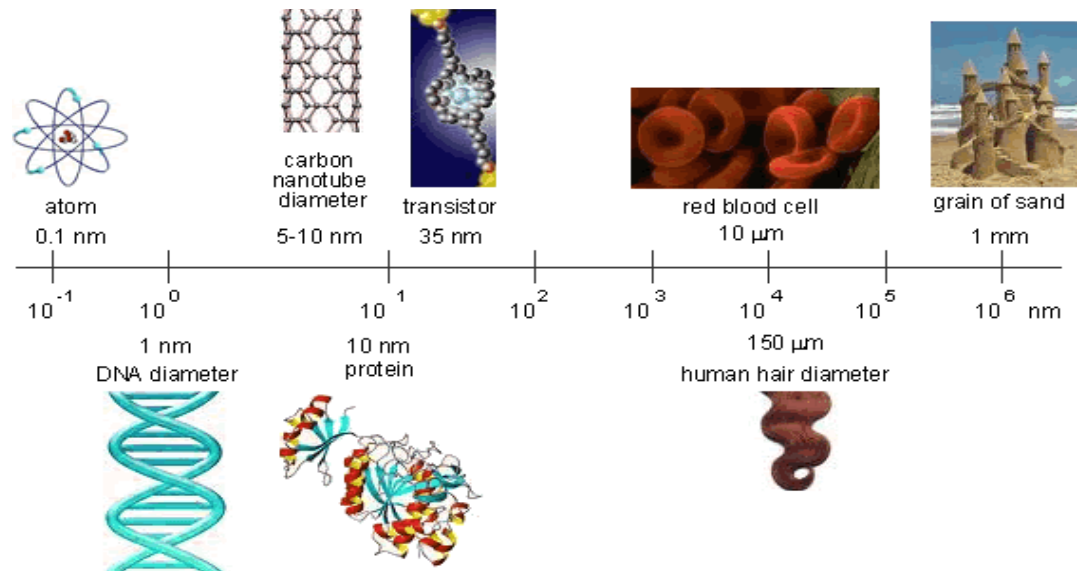


Figure 1.1: The comparison of size with different matters (adapted from: <http://nanoscience.massey.ac.nz/>)

1.3 Nanomaterials

Nanomaterials are not simply another step in the miniaturization of materials. They can be metals, ceramics, polymeric materials, or composite materials. Their defining characteristic is a very small feature size in the range of 1-100 nanometers (nm). The nano-world is in between the scale of atomic and quantum phenomena as well as the scale of bulk materials. At its level, some

material properties are affected by the laws of atomic physics, rather than behaving as traditional bulk materials do. They require very different production approaches. There are several processes to create nanomaterials, classified as ‘top-down’ and ‘bottom-up’ which will be discussed below in detail. Below we outline some examples of nanomaterials:

1.3.1 One-dimension Nanomaterials (1-D)

1.3.1.1 Thin Films, layers and surfaces

One-dimensional nanomaterials such as thin films and engineered surfaces have been used for electronic device manufacture, chemistry and engineering. In the silicon integrated-circuit industry, for example, many devices depend on thin films for their operation, and control of film thicknesses approaching the atomic level is routine. Monolayers (layers that are one atom or molecule deep) are also routinely made and used in chemistry. The formation and properties of these layers are reasonably well understood from the atomic level upwards, even in quite complex layers (such as lubricants). Advances are being made in the control of the composition and smoothness of surfaces, and the growth of films (Smart and Moore, 2005).

Furthermore, the development of electronics using organic compounds has led to nanofilm electronic devices. Such films can be applied in computer monitor

as flat-screen displays. Technically, there are two types of displays being used in this industry which are thin-film transistor liquid-crystal display (TTF-LCD) and organic light-emitting diodes (OLEDs). With the aid of this nanotechnology, a thinner, lighter, and more flexible screen can be produced when the bank of transistors is a film of organic material of 20 nm thick instead of a 2 mm thick layer of silicon (Smart and Moore, 2005).

Engineered surfaces with tailored properties such as large surface area or specific reactivity are used routinely in a range of applications such as in fuel cells and catalysts. The large surface area provided by nanoparticles, together with their ability to self assemble on a support surface, could be of use in all of these applications(Smart and Moore, 2005).

1.3.2 Two-dimensional Nanomaterials (2-D)

1.3.2.1 Carbon Nanotubes

Two-dimensional (1D) nanostructures such as carbon nanotubes and semiconductor nanowires have received considerable attention due to their potential applications in electronic, optical and energy conversion devices. The electrical, mechanical properties as well as thermal properties have been investigated at a single nanotube level. However, most of the studies only include estimating the thermal properties of carbon nanotubes from the experiments of micrometer-millimeter-sized mats of carbon nanotubes (Zhang *et al.*, 2006).

Carbon nanotubes (CNTs) were first discovered by Sumio Iijima in 1991. It is produced by rolling a graphene (a single sheet of graphite) sheet (Pradeep, 2008) and is thin cylinders of carbon atoms that are both mechanically strong and highly conducting (Atkins and Paula, 2006). There are two kinds of CNTs which are single-walled nanotube (SWNT) and multi-walled nanotube (MWNT) which were shown in Figure 1.2. Single-walled nanotubes have diameters of about 1 nm, and lengths of the order of 10^{-6} m. These tubes are capped at each end by half of fullerene-type structure and have remarkable properties that can be used for a variety of high performance application because they are very strong mechanically, flexible and can conduct electricity extremely well (Tang *et al.*, 2001). Furthermore, they can absorb 100 times their volume of hydrogen and hence could be applied as a safe storage medium of hydrogen for fuel cells (Silberberg, 2009). A multi-walled nanotube (MWNT) consists of several concentric SWNTs and its diameter varies between 2-25 nm (Atkins and Paula, 2006).

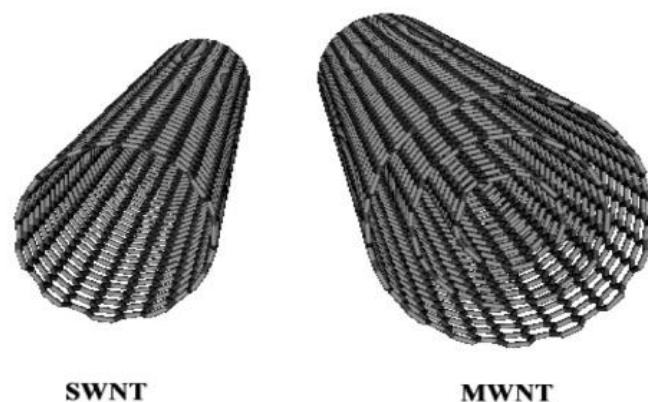


Figure 1.2: Molecular structures of a single-walled carbon nanotube (SWNT) and of a multi-walled carbon nanotube (MWNT). (adapted from http://www-ibmc.ustrasbg.fr/ict/vectorisation/nanotubes_eng.shtml)

1.3.2.2 Nanowires

Nanowires are ultra fine wires or linear arrays of dots with lengths of several micrometres and diameters of less than 20 nm (Have, 2007), formed by self-assembly. The synthesis of nanowire, nanometer-sized atomic assemblies that conduct electricity, is a major step in the fabrication of nanodevice (Atkins and Paula, 2006). Semiconductor nanowires made of silicon and indium phosphides have demonstrated remarkable optical, electronic and magnetic characteristics for example; silica nanowires can bend light around very tight corners. Nanowires have potential applications in high-density data storage; either as magnetic read heads or as patterned storage media, electronic and opto-electronic nanodevices. The preparation of these nanowires relies on sophisticated growth techniques, which include self assembly processes, where atoms arrange themselves naturally on stepped surfaces, chemical vapour deposition (CVD) onto patterned substrates, electroplating or molecular beam epitaxy (MBE). The ‘molecular beams’ are typically from thermally evaporated elemental sources.

1.3.3 Three-dimensional Nanomaterials (3-D)

1.3.3.1 Quantum dots

Quantum dots also known as nanocrystals which are specific type of semiconductor. Quantum dots are sized a few nanometers in diameter and typically containing 10^3 to 10^5 atoms and exhibit quantum-size effects (Atkins

and Paula, 2006). Due to their electrical characteristics, they are electrically tunable. The electrical conductivity of semiconductors can change due to external stimulus such as voltage or exposure to light, etc. As quantum dots have such a small size they show different properties as compare to bulk material. Quantum dots are highly light absorbing, luminescent nanoparticles whose absorbance onset and emission maximum shift to higher energy with decreasing particle size. This is due to the large band gap of the nano-sized metal in its electron orbital as compared to the bulk ones. Figure 1.3 has shown that band-gap energy depends on the composition of the semiconductors as well as the size.

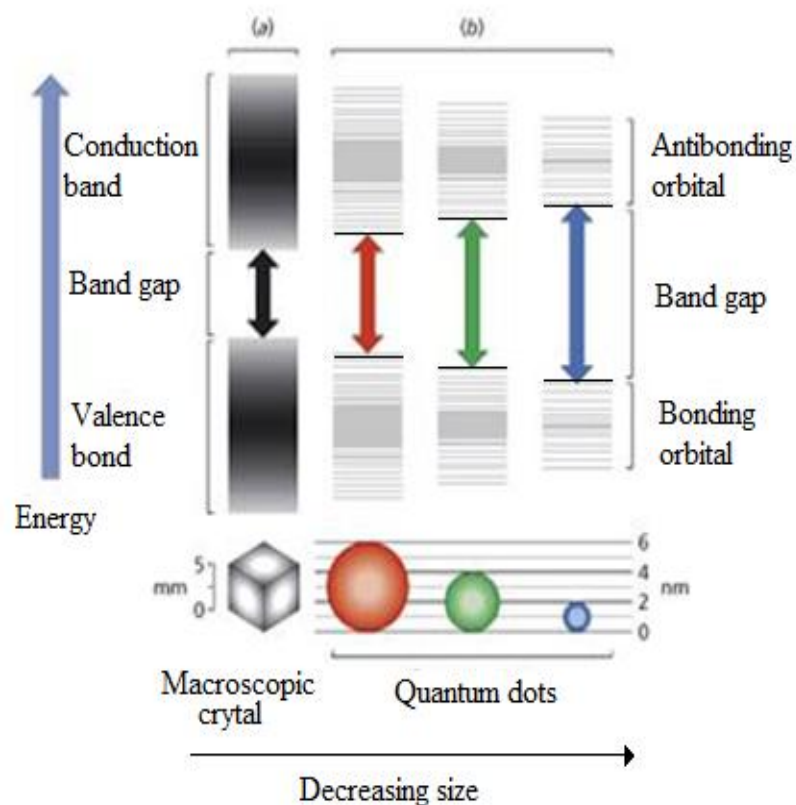


Figure 1.3: The band diagram for nano-sized crystals of semiconductor (quantum dots) (adapted from: <http://www3.imperial.ac.uk/>)

If semiconductor particles are made small enough, quantum confinement effects are observed and its energy level spacing of a nanocrystal exceeds kT (where k is Boltzmann's constant and T is temperature). When Energy differences more than kT which limit the energies at which electrons and holes (the absence of an electron) can exist in the particles. As energy is related to wavelength (or colour), this means that the optical properties of the particle can be finely tuned depending on its size. Thus, particles can be made to emit or absorb specific wavelengths (colours) of light, merely by controlling their size which was shown in Figure 1.4. Recently, quantum dots have found applications in composites, solar cells and fluorescent biological labels (for example to trace a biological molecule) which use both the small particle size and tune able energy levels (Bera *et al.*, 2010).

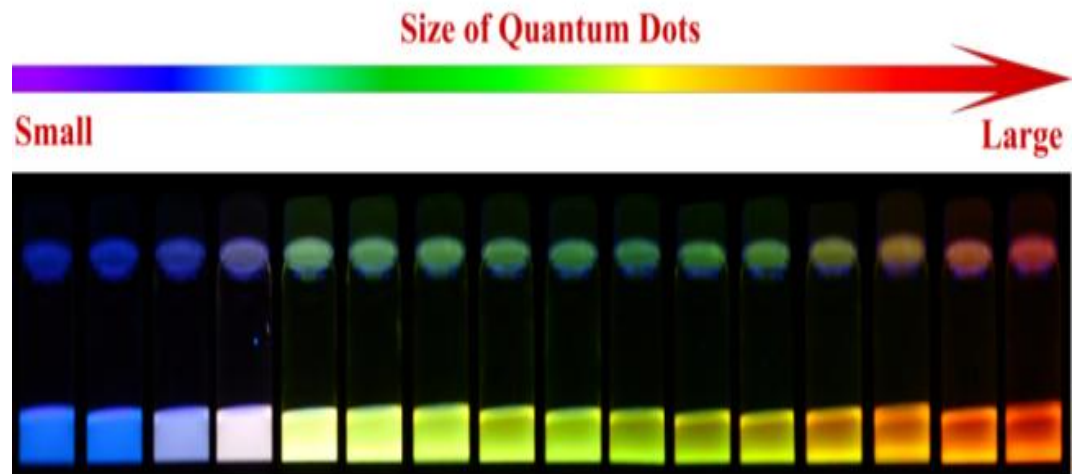


Figure 1.4: Colloidal quantum dots irradiated with a UV light. Different sized quantum dots emit different color light due to quantum confinement. (adapted from: <http://www.mdpi.com/1996-1944/3/4/2260/pdf>)

1.3.3.2 Nanoparticles

Nanoparticles are grouped as three-dimensional nanocrystals. They are generally considered to be a number of atoms or molecules bonded together with a radius of less than 100 nm. A nanometer is 10^{-9} m or 10\AA , so particles having radius of about less than and equal to 1000\AA can be considered to be nanoparticles. The crystal structure of the nanoparticles is the same as the bulk structure with somewhat different lattice parameters (Monasi, 2008).

Nanoparticle materials vary depending on their application. Because nanoparticles are invisible to the naked eye, they are usually supplied suspended in a liquid. The color is due to the refraction of light the surface area of the particular nanoparticle reflects. Different sized nanoparticles exhibit different colors based on its surface area. Therefore, it has been known and used for centuries in colour stained glass, ceramic glazes and also colloidal gold particles used to make 'ruby' glass since Roman times. Metal nanoparticles show peculiar optical, electronic and magnetic properties that bulk solid or isolated molecules do not usually exhibit (Capek, 2004). These properties are explained by Atkins and Paula (2008) as the consequences of their size rather than their chemical composition. Figure 1.5 shows that nanocrystals are suspended in water exhibit different colours depending on its size and shape.

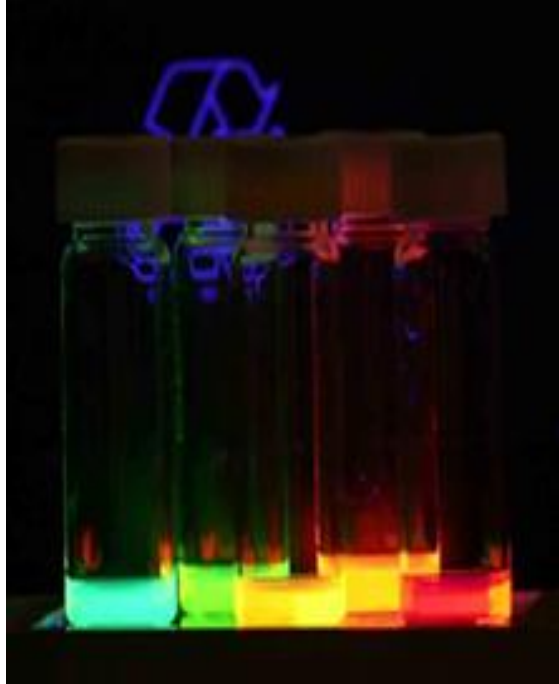


Figure 1.5: Nanoparticles in water suspension exhibit different colours depending on the size and shape (adapted from Bera *et al.*, 2010)

1.3.4 Effect of the Changes in Dimension

1.3.4.1 Changes to the system total energy

Phenomenon of quantum confinement refers to the allowed energy bands become significantly narrower than in an infinite solid when system size decreases. The normal delocalized electronic properties of the solid will become distorted and the electron in this reduced-dimensional system will behave more like the “particle in box”. Total energy of bulk electronic structure will be affected by quantum confinement. It is because thermodynamic stability of the reduced length scales system relative to the normal bulk crystal. It may change the

energetically stable of particular materials. For example, nanoparticles to adopt different crystal structure to normal bulk material. Thus, the changes in the electronic density of states is possible if the crystallographic structure is adopted below critical length scale which results in the reduced of total energy system (Kelsall *et al.*, 2005).

In addition, reduction of system size affect chemical reactivity as well as physical properties such like electrical, optical, thermal and magnetic characteristics due to the changes of the arrangement of the outermost electronic energy levels caused by the reduction of the dimension (Kelsall *et al.*, 2005).

1.3.4.2 Changes to the system structure

The surface area to volume ratio (S/V) and specific surface area of the system will increase when the dimension of a system decreased, significantly for those particles less than 100 nm in diameter. This large surface area will have important implications for the total energy of the system (phenomenon of surface tension of surface energy due to differences bonding). Thus it leads to the stabilisation of metastable structures in nanometer-sized systems, which are different from the normal bulk structure, may induce expansion or contraction of the normal crystalline lattice that could change other material properties (Kelsall *et al.*, 2005).

1.4 Applications of Nanotechnology

As mentioned above, since nanomaterials possess unique, beneficial chemical, physical, and mechanical properties, they can be used for a wide variety of applications. These applications include:

1.4.1 Sunscreens and Cosmetics

Some of the nanosized materials have the properties that they can absorb and reflect ultraviolet (UV) rays and yet are transparent to visible light and so are more appealing to the consumer. For example, nanosized titanium dioxide and zinc oxide are currently used in some sunscreens. However, the use of nanoparticles in cosmetics has raised a number of concerns about consumer safety (Nanowerk, 2011).

1.4.2 Catalysts

Nanoparticles have a high surface area, and hence provide higher catalytic activity as there are more places for other chemical agents to bind and interact for reaction. Hence, it maximizes the possible reactivity, which is the aim for catalyst. Nanotechnologies are enabling changes in the degree of control in the production of nanoparticles, and the support structure on which they reside. It is possible to synthesise metal nanoparticles in solution in the presence of a surfactant to form highly ordered monodisperse films of the catalyst nanoparticles on a surface. This allows more uniformity in the size and chemical structure of the catalyst, which in

turn leads to greater catalytic activity and the production of fewer by-products (Nanowerk, 2011).

1.4.3 Tougher and harder Cutting tools

Cutting tools made of nanocrystalline materials, are much stronger and harder, much more wear-resistant, erosion-resistant, and last longer than their conventional counterparts such as tungsten carbide, tantalum carbide and titanium carbide. Therefore, they enable the manufacturer to machine various materials much faster, thereby increasing productivity and significantly reducing manufacturing costs (Nanowerk, 2011).

1.4.4 Heterogeneous nanostructures and composites

Nanoparticles and rigid nanotubes can be used in composites, materials that combine one or more separate components and which are designed to exhibit overall the best properties of each component with great fracture strength. This multi-functionality applies not only to mechanical properties, but extends to optical, electrical and magnetic ones. Currently, carbon fibres materials and bundles of multi-walled CNTs are used in polymers to control or enhance conductivity, with applications such as antistatic packaging (Nanowerk, 2011).

1.4.5 High-sensitivity Sensors

Sensors made nanocrystalline materials are extremely sensitive to the change in their environment. They employ their sensitivity to the changes in various parameters they are designed to measure. The measured parameters include electrical resistivity, chemical activity, magnetic permeability, thermal conductivity, and capacitance. All of these parameters depend greatly on the microstructure (grain size) of the materials employed in the sensors. A change in the sensor's environment is manifested by the sensor material's chemical, physical, or mechanical characteristics, which is exploited for detection. Typical applications for sensors made out of nanocrystalline materials are smoke detectors, ice detectors on aircraft wings, automobile engine performance sensor, etc. (Nanowerk, 2011).

1.4.6 Therapeutic drugs

Most of these molecular drugs are nanosize, so it becomes more when the drugs are designed specifically to interact with known biological targets. For example, the antidepressant is focused on increasing concentration by blocking or decreasing the destruction of the neurotransmitter molecular (carrier messages) by modifying their binding properties. So, the concentration of it can be restored to normal concentration and hence, treat the depression effectively (Nanowerk, 2011).

1.4.7 Drugs delivery

Bioavailability of drugs is differing to the concentration of drugs. Bioavailability refers to the presence of drug molecules where they are needed in the body. If the drugs delivered directly to the site of a tumour before the tumour spreads to adjacent organs and without interact to others site, chemotherapy could become more effectively. Nanotechnology and nanoscience are useful in increasing bioavailability by encapsulated within the nanoscale cavities inside polymers within the tablet (Nanowerk, 2011).

1.4.8 Optical electronics

Semiconductors with nanoscale dimension can act as light-emitting structures. Since their intensity can color can be chosen, these nano sources are very promising for applications in electronic industry such as flat screen, LED, cellular phone displays and etc. (Nanowerk, 2011).

1.4.9 Transistor

Nanoscale structures can act as transistors and the individual molecules can act as field effect transistors. This reduced the size more than 100 times smaller than those afforded by currently available standard lithography work in silicon. By combining this transistor with memory devices, allows the processors to be further reduced in size (Nanowerk, 2011).

1.5 Fabrication methods

There are numerous ways to produce a nanostructure product. However, there are generally divide into two approaches which are top-down approach and bottom-up approach for synthesis of nano materials which were shown in Figure 1.6. Under controlled conditions, both the top-down and bottom-up approaches can be viewed as different forms of microstructure engineering.

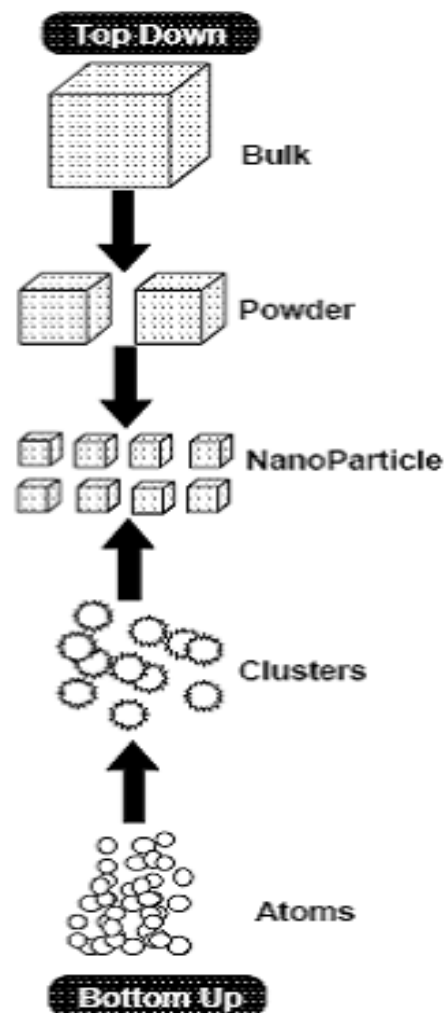


Figure 1.6: Schematic representation of the building up of Nanostructures.

(adapted from: http://www.gitam.edu/eresource/nano/nanotechnology/role_of_bottom_up_and_topdown_a.htm)

1.5.1 Top down approach

The top-down approach is the fabrication method that uses the simple removal or successive cutting of bulky material to reduce the size down to the nano-sized particle or structure. On the other hands, it is actually a miniaturization process of bulky materials. Some of the example methods of top-down approach:

- i. Milling of Attrition
- ii. Machining

1.5.2 Bottom up approach

In the bottom-up approach, it is a method that uses the atoms, molecules and even nanoparticles themselves as the building blocks for the creation of the nanostructure. It means that they build up of a nanostructure material from the bottom: atom by atom, molecule by molecule or cluster by cluster. The properties and functionalities of nanostructured materials produced by this method may possible assist by changing the size of building blocks, controlling their surface and assembly organisation. Some of the example methods of bottom-up approach:

- i. Sol-gel method
- ii. Colloidal dispersion methods
- iii. Vapour phase deposition methods

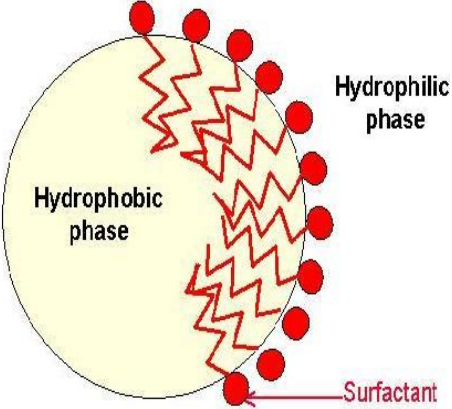
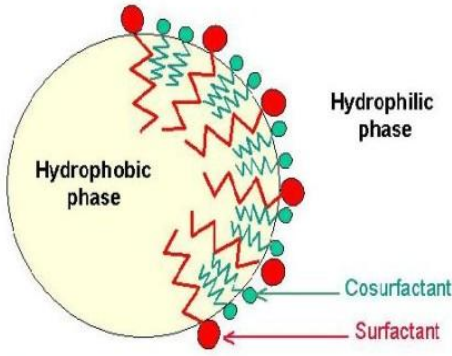
1.5.3 Template growth of nanomaterials

Template growth of nanomaterials is essentially in one of the bottom-up approaches. It is different from others due to utilizing the principle of wet chemistry. In this method, usually will to precipitate or deposit a material and control the growth of nanostructure formed. However, control of the precipitate size can be difficult and sometimes complicated unless some chemicals are added to control the precipitates formed. In this case, the nanoparticles growth can be regulated within self-organised, biological and synthetic organic membranes assemblies such as micelles, microemulsions, liposomes and vesicles.

1.5.3.1 Differences of Microemulsion and emulsion system

Emulsions are defined as the mixture of two or more immiscible liquids by any means of mixing method (macroscopically homogeneous and microscopically heterogeneous). They revert back to two or more phases over time if without the presence of any supporting substance like emulsifier to withhold (Paul and Moulik, 2001). Unlike emulsion, microemulsion-processing method is a soft technique and does not required special instrument or extreme condition (Khiew *et al.*, 2003). They are low viscosity, large interfacial area and having ability to solubilise both aqueous phase and oil-soluble compounds (Paul and Moulik, 2001). Furthermore, the system is stabilised by a surfactant film (Lopez-Quintela, 2003). Table 1.1 shows the comparison of emulsion and microemulsion.

Table 1.1: Comparison of emulsion and microemulsion

<p align="center">Emulsions (Macroemulsions)</p>	<p align="center">Microemulsions</p>
 <p>Surfactant: Forms the interfacial film</p>	 <p>Surfactant: Forms the interfacial film CoSurfactant: Ensures flexibility of interfacial layer => reduces the interfacial tension</p>
<ul style="list-style-type: none"> • Consist of roughly spherical droplets of one phase dispersed into the other. 	<ul style="list-style-type: none"> • They constantly evolve between various structures ranging from droplet like swollen micelles to bicontinuous structure.
<ul style="list-style-type: none"> • Droplet diameter: 1 – 20 μm. 	<ul style="list-style-type: none"> • 10 – 100 nm.
<ul style="list-style-type: none"> • Most emulsions are opaque (white) because bulk of their droplets is greater than wavelength of light and most oils have higher refractive indices than water. 	<ul style="list-style-type: none"> • Microemulsions are transparent or translucent as their droplet diameter are less than $\frac{1}{4}$ of the wavelength of light, they scatter little light.
<ul style="list-style-type: none"> • They may remain stable for long periods of time, will ultimately undergo phase separation on standing to attain a minimum in free energy. They are kinetically stable but thermodynamically unstable. 	<ul style="list-style-type: none"> • More thermodynamically stable than macroemulsions and can have essentially infinite lifetime assuming no change in composition, temperature and pressure, and do not tend to separate.
<ul style="list-style-type: none"> • Require intense agitation for their formation. 	<ul style="list-style-type: none"> • Generally obtained by gentle mixing of ingredients.

(adapted from: <http://www.pharmainfo.net/reviews/microemulsions-novel-drug-delivery-vehicle>)

1.6 CuSe and Its application

In the past decades, semiconductor nanomaterials have received broad attentions due to their novel electronic, optical, photoelectric and thermoelectric properties. As an important semiconductor, copper selenide (CuSe) with nanostructure has potential applications in various fields, such as optical filter, highly efficient solar cells, super ionic conductors and thermoelectric converters, electro-optical devices, photo-thermal conversion, electro-conductive electrodes, and microwave shielding coating. These materials are semiconductors with p-type conductivity (Zainal *et al.*, 2004). Thus, many studies about the preparation and characterisation of CuSe nanostructures have been reported. It may be more important to find out the properties of CuSe nanostructures because the applications of CuSe can be derived from these findings (Wei *et al.*, 2007).

Copper selenide is a metal chalcogenide semiconductor with a wide range of stoichiometric compositions and also with various crystallographic forms for each of these compositions. The synthesis of this material in thin film form has been described by using different deposition method such as chemical bath deposition (CBD) selenisation, flash evaporation, vacuum evaporation and spray method, etc.. Copper selenide exists in widely different crystallographic modifications even at room temperature such as (orthorhombic, monoclinic and cubic) forms, depending on the method of preparation.

Objectives

The objectives of this project are:

1. To synthesise CuSe nanoparticles using emulsion technique.
2. To characterise the CuSe nanoparticles using X-Ray Diffractometer, UV-Vis Spectrophotometer and Fluorescence Spectrophotometer.
3. To investigate the effect of concentration of reducing agent (NaBH_4), various stirring period and autoclaved period on the formation of CuSe nanoparticles.

CHAPTER 2

LITERATURE REVIEW

2.1 Microemulsion and the Formation of Micelles Structure

Microemulsion has been verified as an effective approach to obtaining ultrafine inorganic particles (Xu and Li, 2003). One of the powerful techniques for obtaining the ultrafine particles is based on the use of microemulsions in order to control the growth of the particles (Capek, 2004)

A stabiliser (emulsifier) is a molecule that processes both polar and non-polar moieties. In diluted water (or oil) solutions, emulsifier dissolves and exists as monomer, but when its concentration exceeds a certain minimum, the critical micelle concentration (CMC), the molecules of emulsifier associate spontaneously to form aggregates-micelles. Micelles are responsible for many of the processes such as enhancement of the solubilisation of organic compounds in water (oil-in-water (o/w) emulsion) or hydrophilic compounds in the oil phase (water-in-oil emulsion). The formation of o/w or w/o micelles is driven by strong hydrophilic interactions of the hydrophobic tail of the emulsifier molecule (o/w micelle) or by hydrophilic interactions of the polar head of the emulsifier molecule (w/o micelle). In some cationic emulsifiers, the aggregation numbers are

quite small, there is no real identifiable CMC, and the aggregation number increases continuously with increasing solute concentration (Capek, 2004).

A normal micelle is known as oil-in-water (o/w) micelle while inverse micelle is known as water-in-oil (w/o) micelle. The formation of o/w micelle is driven by the strong hydrophobic interactions of the surfactant hydrophobic tail whereas the formation of w/o micelle is driven by the hydrophilic interactions of the surfactant polar head. In the latter case, the hydrophilic groups of the surfactant will point into the centre of the aggregate while the hydrophobic tails will extend out to the organic solvent phase. Figure 2.1 shows the structure of inversed micelle and normal micelle.

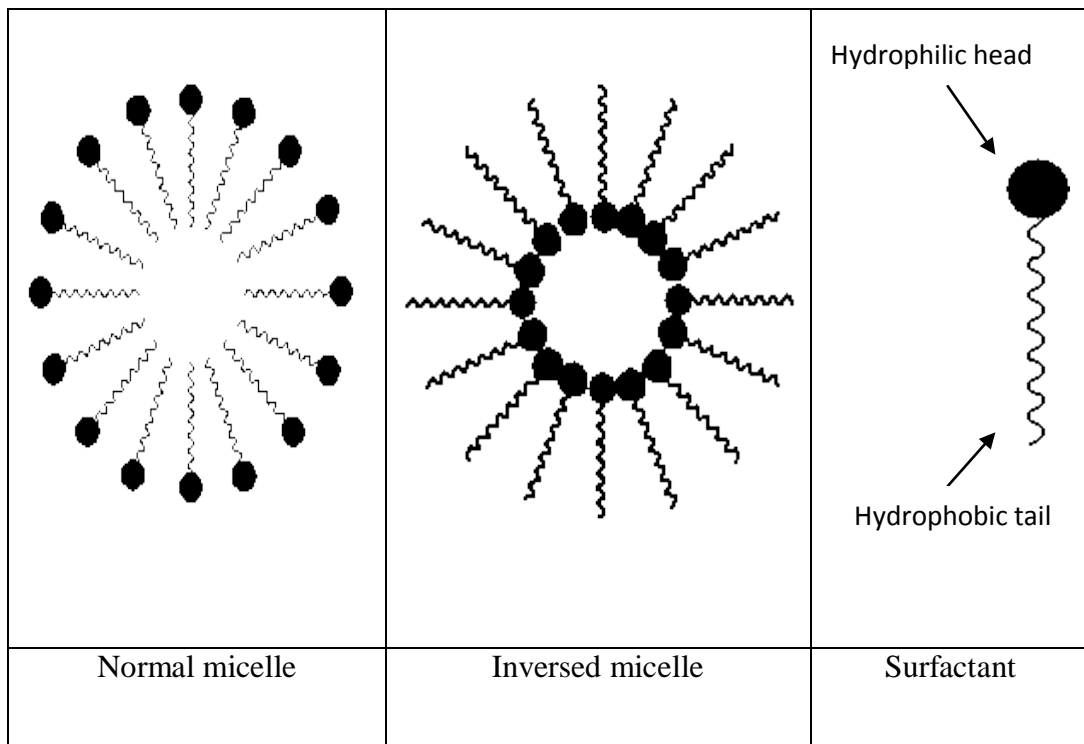


Figure 2.1: Structure of inverse micelle and normal micelle

w/o microemulsion solutions are mostly transparent liquid media where the nanosized water droplets are dispersed in the continuous oil phase and stabilised by the surfactant molecule at the interface. Synthesising metal nanoparticles by using this reverse micelle method provides a favourable microenvironment for controlling the chemical reaction, thus being able to obtain a narrow size distribution of nanoparticles. However, the nanoparticles will not form below the critical micelle concentration (CMC) of various surfactants. However, oil in water emulsion which oil is present as the dispersed phase and water as the dispersion medium (continuous phase). Figure 2.2 shows a general mechanism for formation of metal nanoparticles via w/o and o/w microemulsion (Capek, 2004).

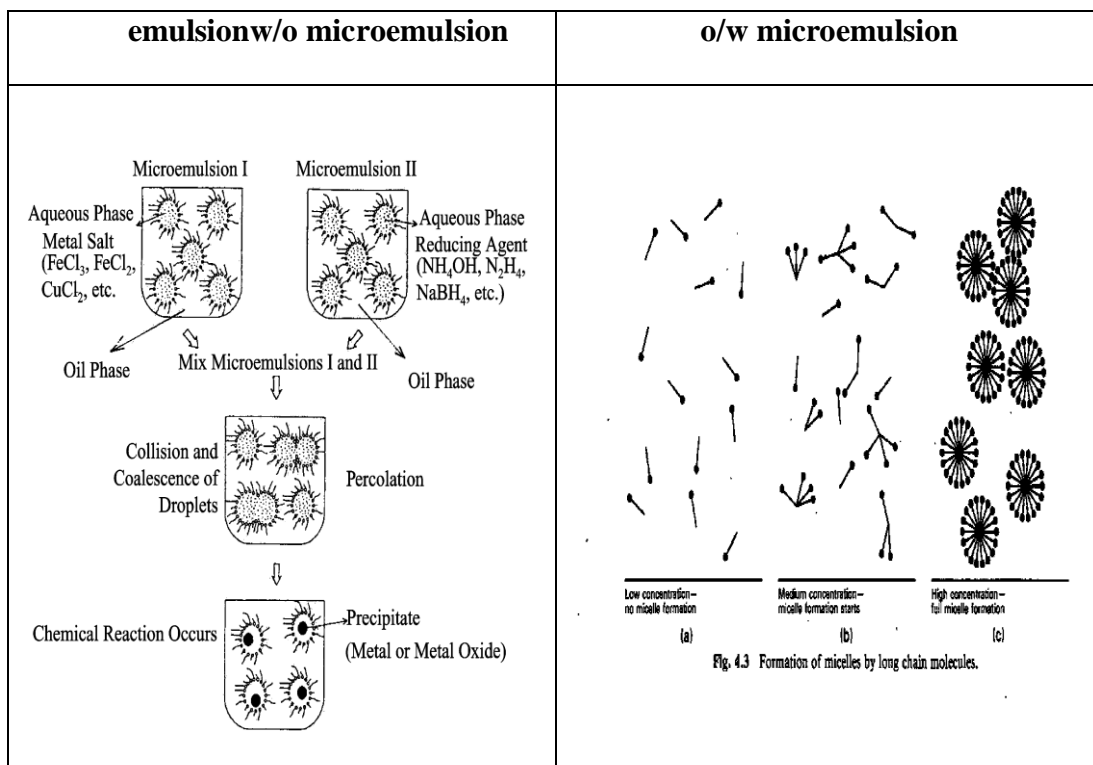


Figure 2.2: Comparison between water in oil emulsion and oil in water Emulsion (adapted from: Capek, 2004)

In the study of Tamura *et al.*, an inverse micelle made up by the ternary systems of alkane (toluene, n-heptane, AOT)/water have an advantage where the spheroidal and monodisperse aggregates are formed and the water is readily solubilised in the polar core, forming a 'water pool' characterised by the ratio of water to surfactant concentration, also known as 'W'. The size of nanoparticles is believed to be depended on the 'W' value where the diameter of the nanoparticles shall increase proportionally to the 'W' value. Besides that, a narrow size distribution of nanoparticles is more easily obtained through this method as compared to the precipitation method (Capek, 2004).

2.2 Effect of CTAB on the formation of nanoparticle

Cetyl trimethylammonium bromide ($C_{16}H_{33}-(CH_3)_3-N^+Br^-$, CTAB) can be acts as surfactant because of its reverse micellar systems which show extraordinarily more solubilisation capacity of high concentration aqueous salt solution than AOT-based systems. It provides a very flexible film, which gives rise to a high exchange dynamic of the micelles (Capek, 2004).

Nanoparticles size can be affected by changing the concentration of the reactants, metal salt and reducing agent. The final Ni nanoparticle size in a water/CTAB/n-hexanol microemulsion was changed due to the effect of different concentration of the starting materials used. The size of Ni nanoparticles decreases with the increase of hydrazine concentration and then approaches to a

constant NiCl concentration value. This is due to the reduction rate on the nucleation which occurs as collisions between several atoms. Once the nuclei are formed, the growth would be superior to nucleation. Nanoparticles would be monodisperse if the nuclei were formed almost at the same time and grew at the same rate. Hence, the number and size distribution of the obtained particles will be determined by the number of nuclei formed at the very beginning (Capek, 2004).

The reduction rate is slow, and only few nuclei are formed at the initial period of the reduction due to the low concentration of hydrazine. The collision between nuclei and atoms formed at a latter period, therefore larger particles are obtained. However, the enhanced reduction rate favours the generation of higher number of nuclei, and leads to smaller Ni nanoparticles since the concentration of hydrazine is higher. However, the reduction is faster than the nucleation when the concentration ratio of hydrazine to NiCl is large enough. The number of nuclei is held constant up to the certain degree of hydrazine concentration and the nucleation rate is not further raised. Due to this reason, the size of the nanoparticles remains constant (Capek, 2004).

Synthesising of ZrO_2 - Y_2O_3 nanoparticles which was obtained in a CTAB/hexanol/water microemulsion. The report illustrated that nanoparticle size distribution is narrowed down in two cases, increasing water content at fixed surfactant concentration or decreasing the surfactant content at fixed water. Both

cases led to larger droplets. More nuclei were formed in reverse micelles when there are a huge number of metallic ions existing in a large droplet.

The increasing of the water content will lead to the increasing droplet size; the surfactant film becomes thinner, thus accelerating the exchange process. A uniform nucleation and growth process will formed due to the higher exchange rate. However, the decreasing of water content lead to smaller sizes, nucleation only occurs in a little number of micelles at the very beginning of the precipitation reaction, because they do not contain enough metal ions to form a critical nucleus. As a result, due to diffusion, new nuclei will form as a function of time. Particles already existing and newly emerging will grow at a different rate, causing a broad size distribution (Capek, 2004).

2.3 Water/oil volume ratio effects on the formation of CuInSe₂

The volume ratio plays a very important role in the formation of nanoparticles. Figure 2.3 (a), (b), and (c) show the diffraction patterns with the *W/O* volume ratios for 1:5, 1:10, and 1:15 and the X-ray diffraction patterns of the powders prepared via the microemulsion-mediated solvothermal route at 200 °C for 3 h (Lu *et al.*, 2010).

When the *W/O* volume ratio was 1:5, selenium was found to exist as the main phase. The CuInSe_2 and CuSe phases were observed Figure 2.3 (a). As the *W/O* volume ratio was adjusted to 1:10, the CuInSe_2 compound was formed as the major phase. A small amount of selenium was also observed as seen in Figure 2.3 (b). When the *W/O* volume ratio was 1:15, the pure CuInSe_2 phase was successfully synthesised. The resulting diffraction pattern in Figure 2.3 (c) was in good agreement with the standard CuInSe_2 pattern (ICDD card no. 89-56490). During the reaction process, excess copper ions will easily react with Se ions to form CuSe (Lu *et al.*, 2010).

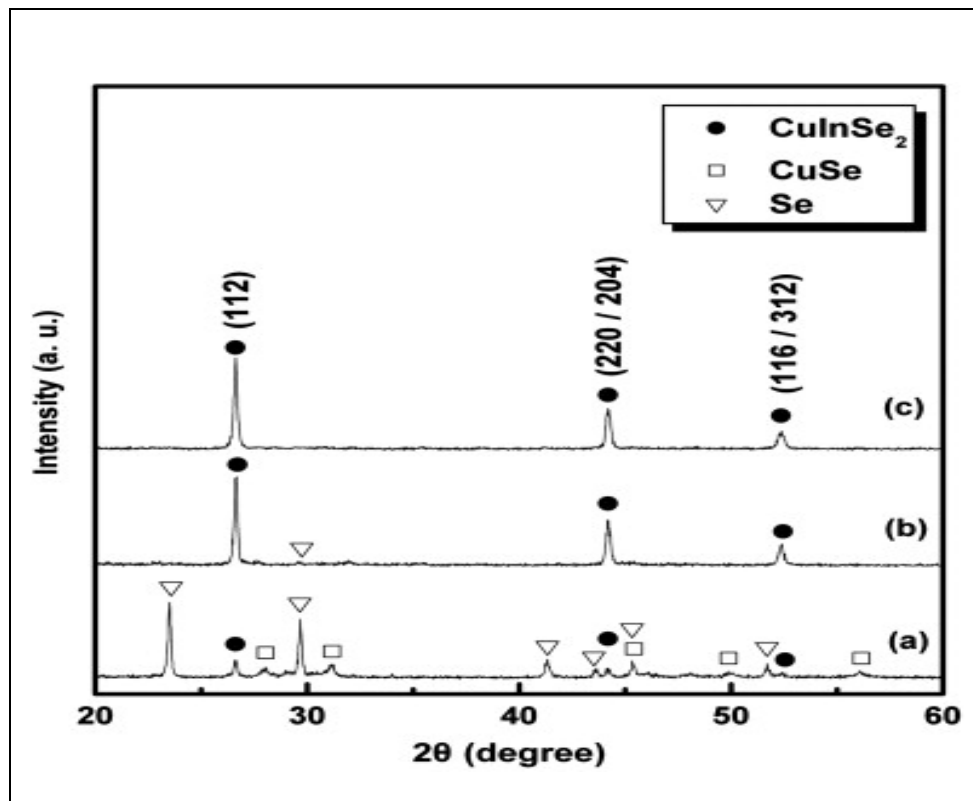


Figure 2.3: XRD patterns of CuInSe_2 powders prepared at 200 °C for 3 h with the *W/O* volume ratios of (a) 1:5, (b) 1:10, and (c) 1:15 in the microemulsion-mediated solvothermal process (Lu *et al.*, 2010).

The above result indicated that the formed phase was significantly influenced by the w/o volume ratio. The system was unstable when the w/o volume ratios were 1:5 and 1:10. The size of the micelles in the unstable microemulsion system was not uniform. The different-sized micelles probably caused the reactants to distribute non-homogeneously, thereby resulting in the formation of secondary phases. It produces good dispersion of the reactants in the solution while increasing in the amount of oil phase resulted in enhancing the microemulsion system stability. In the above three kinds of w/o volume ratios, the pure CuInSe₂ phase was formed when the w/o volume ratio was 1:15 only. (Lu *et al.*, 2010).

2.4 Duration effects on the microstructures of CuInSe₂ powders

From Figure 2.4 and 2.5, it can be observed that the duration effect is very important in synthesising pure and nano-sized particles. When the reaction duration was 30 min to synthesis CuInSe₂ nanoparticles, a small amount of CuSe and selenium impurity phases existed in the sample and only a little amount of CuInSe₂ nanoparticles achieved which was shown in Figure 2.4 (a). After heating for 1 h, the amount of CuInSe₂ increased with the corresponding decrease in the amounts of CuSe and selenium Figure 2.4 (b). In addition, when the reaction time was prolonged to 3 and 5 h, a pure CuInSe₂ compound was formed Figure 2.4 (c) and (d). Figure 2.4 illustrates the X-ray diffraction patterns of CuInSe₂ samples prepared at 200 °C for different reaction times (Lu *et al.*, 2010).

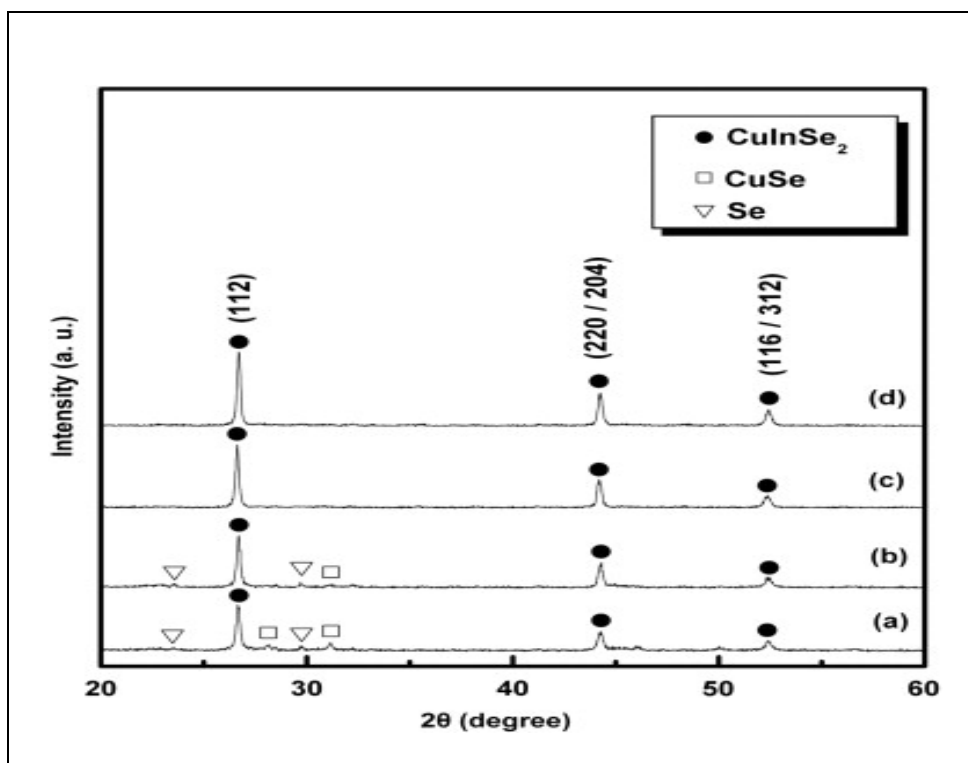


Figure 2.4: XRD patterns of CuInSe_2 powders prepared at 200 °C for (a) 30 min, (b) 1 h, (c) 3 h, and (d) 5 h with the W/O volume ratio of 1:15 in the microemulsion-mediated solvothermal process (Lu *et al.*, 2010).

In fact, it needs at least 15 h for preparing single-phased CuInSe_2 powders via the conventional solvothermal route. In this study, the preparation time for the pure CuInSe_2 phase in the microemulsion-mediated solvothermal process was significantly shortened to 3 h. Therefore, the distances between the constituent reactants are greatly decreased within tiny micelles. The reactants can react with each other in the micelles within a short time. In the microemulsion-mediated solvothermal process, cyclohexane was used as the continuous phase. Because cyclohexane has high thermal conductivity, the heat transfer efficiency was

increased. This also leads to an increase in the reaction rate, thereby reducing the required reaction durations (Lu *et al.*, 2010).

Figure 2.5 shows TEM micrographs of CuInSe₂ powders prepared at 200 °C for various reaction times. The particles sizes were around 5 nm when the reaction durations were 30 min and 1 h which are shown in Figure 2.5 (a) and (b). Prolonging the reaction time to 3 and 5 h increased the particle sizes of the derived samples to 10 and 15 nm, respectively Figure 2.5 (c) and (d). To conclude, the sizes of the derived powders increased with increase in reaction duration (Lu *et al.*, 2010)

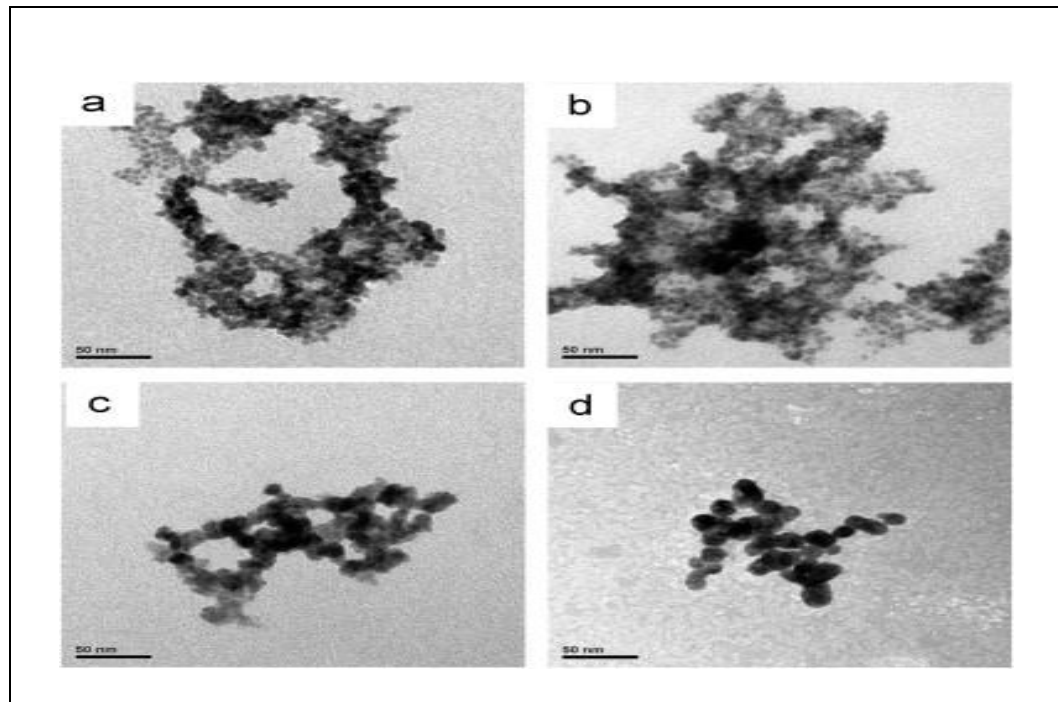


Figure: 2.5: TEM micrographs of CuInSe₂ powders prepared at 200 °C for (a) 30 min, (b) 1 h, (c) 3 h, and (d) 5 h with the *W/O* volume ratio of 1:15 in the microemulsion-mediated solvothermal process (Lu *et al.*, 2010).

2.5 Effect of reaction temperature on the microstructures of CuInSe₂ powders

CuInSe₂ powders were synthesised via the developed microemulsion-mediated solvothermal process at different temperatures for 3 h. The X-ray diffraction patterns of the prepared samples are shown in Figure 2.6. The main product in the sample was CuSe while only a small amount of CuInSe₂ and selenium coexisted with CuSe in the sample when the reaction temperature was 160 °C which are shown in Figure 2.6 (a) (Lu *et al.*, 2010).

However, CuInSe₂ started to form as the major phase in the products when the reaction temperature up to 180 °C which are shown in Figure 2.6 (b). Further raising the reaction temperature to above 200 °C, single-phased CuInSe₂ was successfully produced Figure 2.6 (c) and (d). The diffraction intensity of CuInSe₂ was increased with an increase in reaction temperatures (Lu *et al.*, 2010).

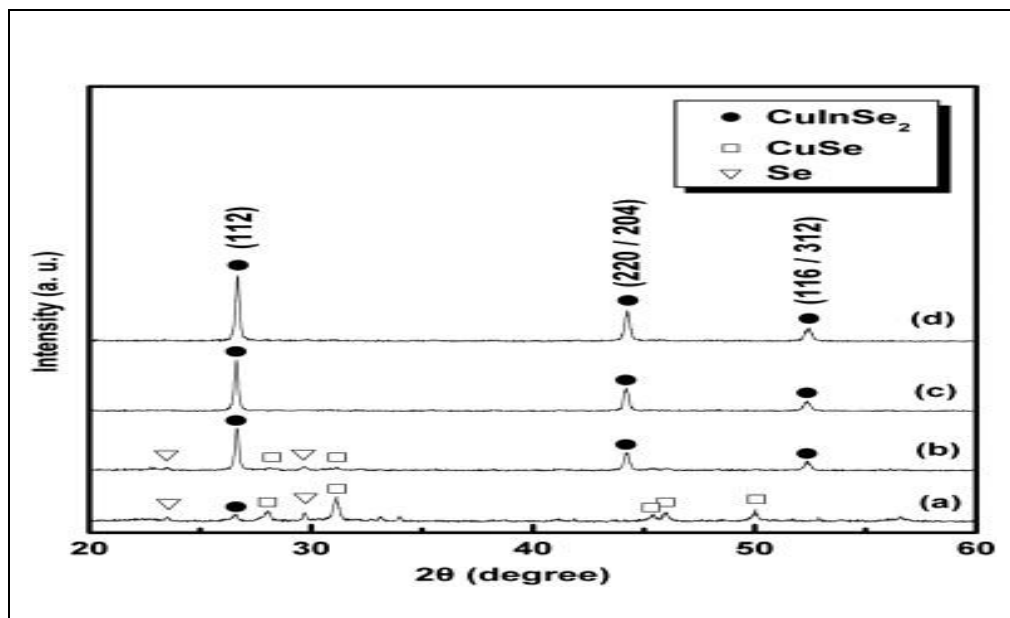


Figure 2.6: XRD patterns of CuInSe_2 powders prepared at (a) 160 °C, (b) 180 °C, (c) 200 °C, and (d) 220 °C for 3 h with the W/O volume ratio of 1:15 in the microemulsion-mediated solvothermal process (Lu *et al.*, 2010).

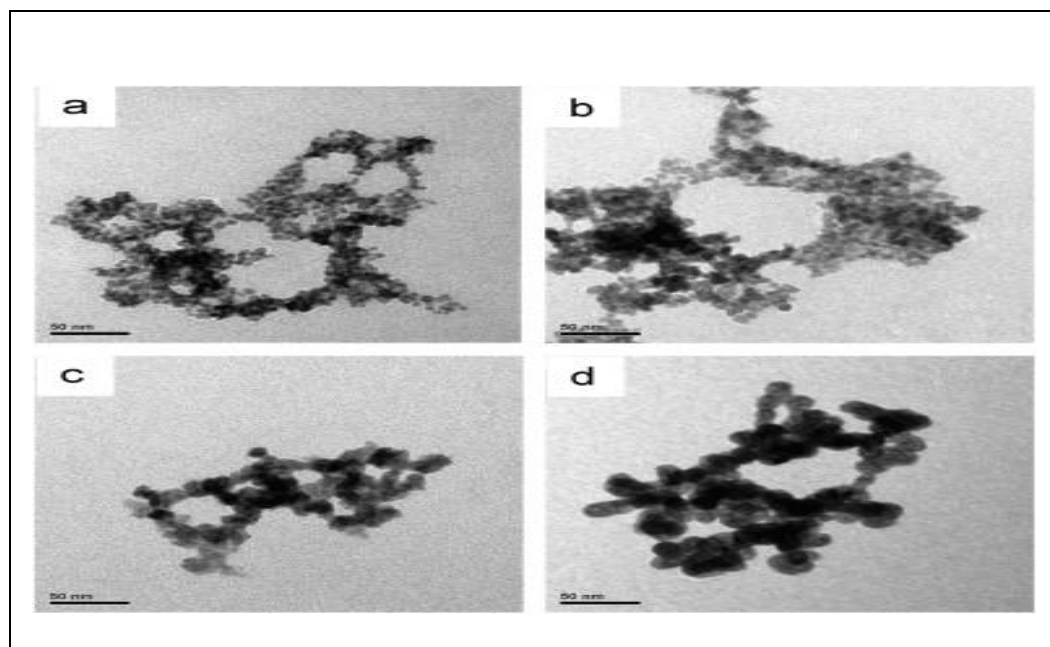
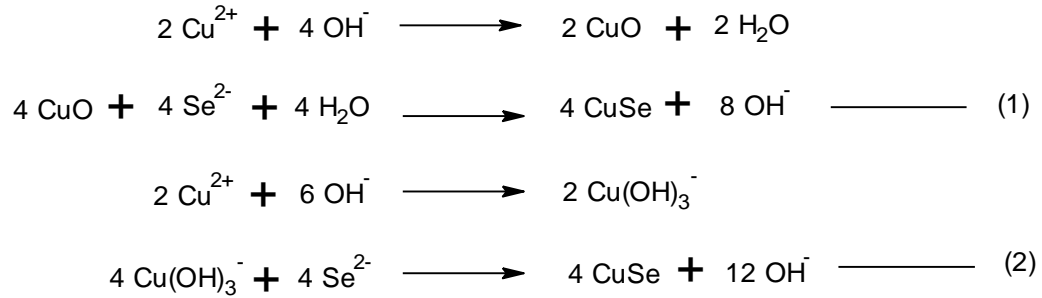


Figure 2.7: TEM micrographs of CuInSe_2 powders prepared at (a) 160 °C, (b) 180 °C, (c) 200 °C, and (d) 220 °C for 3 h with the W/O volume ratio of 1:15 in the microemulsion-mediated solvothermal process (Lu *et al.*, 2010).

TEM photographs of CuInSe₂ powders prepared at various temperatures are shown in Figure 2.7. The obtained results reveal that the microemulsion-derived powders exhibited uniform and spherical morphology. Figure 2.7 (a) shows the particle size of the 160 °C-synthesized sample was around 5 nm. On increasing the reaction temperature to 180 °C, particles with a diameter of 7 nm were obtained which is shown in Figure 2.7 (b). Further increasing the reaction temperature to 200 and 220 °C, the particle sizes of CuInSe₂ powders were increased to 10 and 15 nm, respectively which is shown Figure 2.7 (c) and (d). To conclude, the sizes of the prepared CuInSe₂ powders increased with increasing in reaction temperature (Lu *et al.*, 2010).

2.6 Effect of reducing agent and the growth mechanism

A growth mechanism of nanoplates is proposed in the below equation (1) and (2). Se source was reduced by N₂H₄; this highly reactive Se can be easily converted into Se²⁻, which results in a high monomer concentration. In the initial step, hydrazine hydrate complexes with Cu²⁺ and forms a transparent soluble complexes solution, which effectively decreases the concentration of Cu²⁺ and avoids the precipitation of CuSeO₃, thus provides a more homogenous solution environment for the reaction. The chemical reaction involved in the entire synthesis of nanoplates can be formulated as follows:



Se^{2-} is released slowly and interacts with surplus N_2H_4 to form the molecular precursor immediately. The application of N_2H_4 as the coordination agent is determinable for the phase of the products. Compared with the CuO deposit Equation (1), it is easier for the Cu(OH)_3^- Equation (2) to release Cu^{2+} , which can facilitate the growth of nanoparticles under non-equilibrium kinetic growth conditions with a high monomer concentration. The above result reveals that N_2H_4 acts as a solvent, favors the formation of copper selenide nanostructure. To conclude, the appropriate ratio of reducing volume plays a critical role in the formation of nanoplates (Kumar *et al.*, 2010).

2.7 Lattice constant for the geometry of hexagonal nanoparticles

Copper selenide was prepared by the reactions of elements of pure copper (99.999%) and selenium (99.999%). The mixtures of equal mol of Cu and Se were loaded into a quartz ampoule. The quartz ampoule was then sealed under a pressure of 2.7×10^{-3} Pa and kept inside a rotating furnace. The samples were heated to 1326 K and were allowed to rotate for about 3 days and then cooled to

295 K. The products from these steps were used for evaporation. The structural analysis was made using a X-ray diffractometer (XRD) [Shimadzu XRD-6000] using $\text{CuK}_{\alpha 1}$ radiation in the scanning angle (2θ) from 10° to 70° .

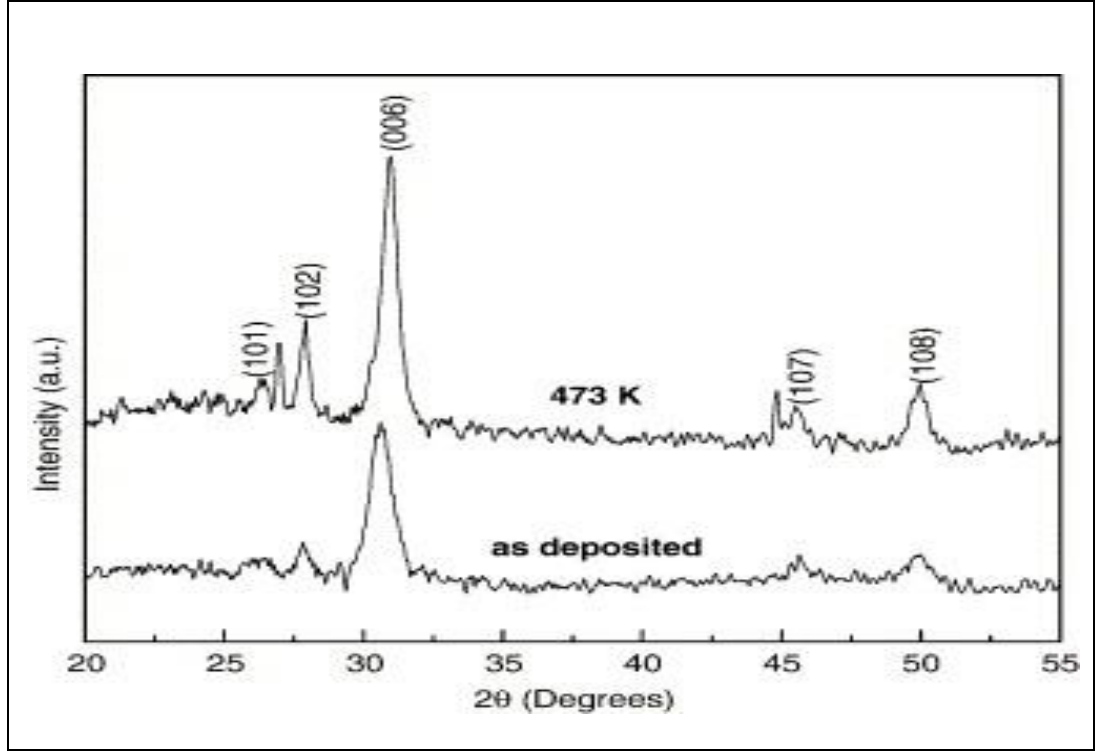


Figure 2.8: X-ray diffractogram of as-deposited and 473 K annealed CuSe Films (Peranatham *et al.*, 2006).

Figure 2.8 shows the X-ray diffraction pattern of a vacuum evaporated CuSe thin film of a typical thickness 271 nm deposited onto a glass substrate at room temperature and then annealed at 473 K. The structure of the film is found to be hexagonal with a predominant orientation along the (006) plane (JCPDS: 34–171) (Peranatham *et al.*, 2006). The lattice constant for the hexagonal structure is determined by the following equation,

$$\frac{1}{d^2} = \frac{4}{3} \frac{h^2 + hk + k^2}{a^2} + \frac{l^2}{c^2}$$

2.8 Physical, optical and electrical properties of copper selenide (CuSe) thin films deposited by solution growth technique at room temperature

Thin films of copper selenide have been grown by solution growth technique using selenium powder, sodium sulphite, cupric chloride and ammonia. A solution of sodium selenosulphate was prepared by refluxing 100 ml of 0.4M sodium sulphite with selenium powder for about 5–6 h. This solution will contain excess of sodium sulphite which prevents the oxidation of selenide to selenium. Reaction bath contains 10 ml 0.1M $\text{CuCl}_2 \cdot 2\text{H}_2\text{O}$, 0.8 ml of 30% NH_3 aqueous, 10 ml of freshly prepared solution of Na_2SeSO_3 in 100 ml beaker and the rest distilled water to make the volume to 50 ml. On controlling the pH value at 10.0, uniform films of copper selenide have been obtained on glass substrates. Well-cleaned glass substrates were then immersed vertically into the deposition bath against the wall of the beaker containing the reaction mixture. The deposition was allowed to proceed at room temperature for different time durations. After deposition, the glass microslides were taken out from the bath, washed with de-ionized water and was dried in air. The preparative parameters were optimised, concentration of the reactant solutions (CuCl_2 and Na_2SeSO_3), 0.1 M, pH 10, deposition temperature 300K and deposition time 6 h. Optical analysis was observed according to the above parameter (Gosavi, 2007).

The theory of optical absorption gives the relation between the absorption coefficient and the photon energy, for direct allowed transition as:

$$\alpha h\nu = A(h\nu - E_g)^{1/2} \quad (1)$$

where , A is the constant,

E_g is the band gap,

$h\nu$ is the photon energy.

From Figure 2.9 shows the variation of $(\alpha h\nu)^2$ with $h\nu$. By extrapolating straight line portion of $(\alpha h\nu)^2$ against $h\nu$ plot to $\alpha=0$, the optical band gap energy was found to be 2.03 eV.

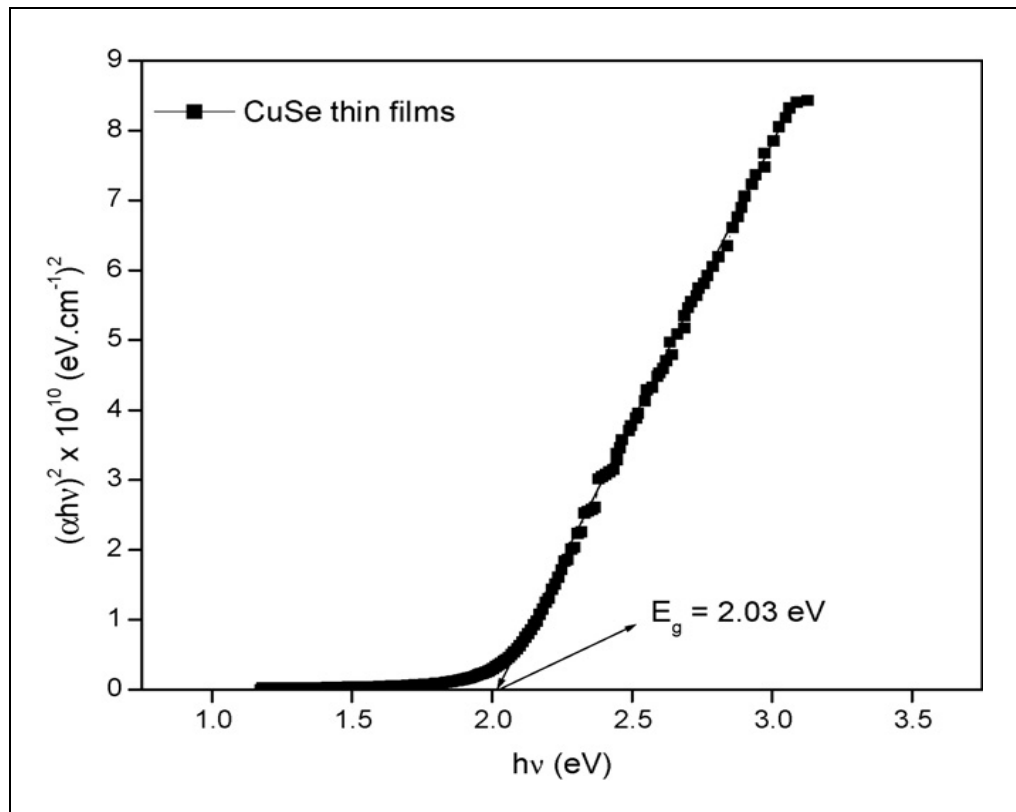


Figure 2.9: Plot of $(\alpha h\nu)^2$ vs. $h\nu$ for CuSe thin films (Gosavi, 2007).

2.9 Optical properties and electrical conductivity studies of copper selenide nanoparticle

Figure 2.10 shows the optical absorption measurements carried out in the spectral range (190–900 nm) for CuSe prepared at 160, 170 and 200 °C. This figure has been shown that there is no sharp absorption edge observed at longer wavelengths. However, a set of sharp absorption peaks was clearly observed at shorter wavelengths due to exciton absorption which formed at low temperature and the confinement was formed at relatively higher temperatures. Furthermore, it can be observed that the absorbance increases with increasing temperature. This may be due to the increase of the particle size and decrease of the inter-distance between CuSe nanoparticles in the solvent causing increased absorbance with increasing temperature (Seoudi *et al.*, 2006).

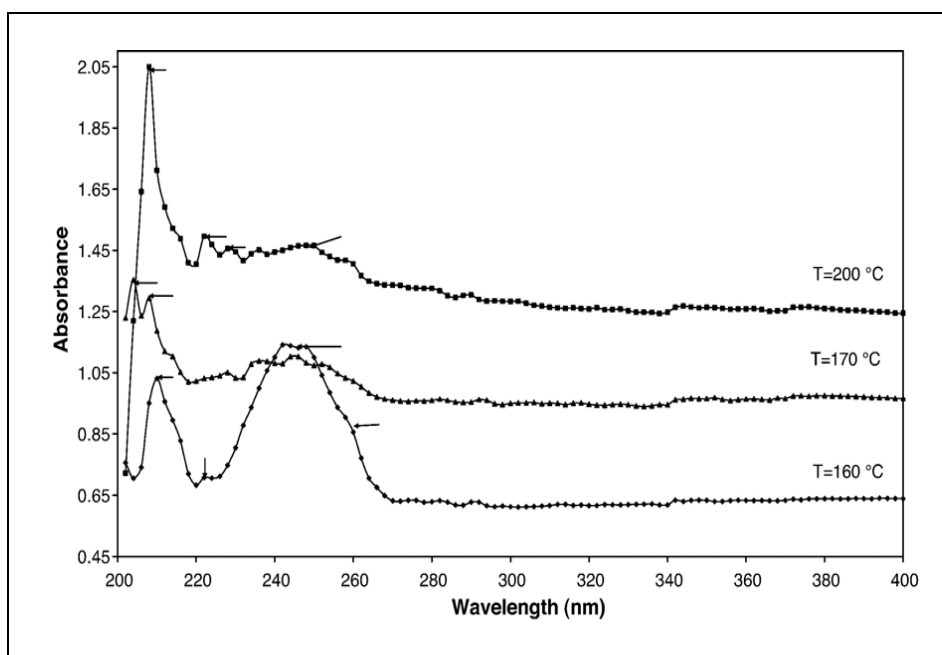


Figure 2.10: The relation between absorbance and wavelength for CuSe prepared at T=160 °C, T=170 °C and T=200 °C dispersed in absolute ethanol (Seoudi *et al.*, 2006).

The optical band gap E_g , can be determined from the experimental values of the absorption coefficient, α as a function of the photon energy, $h\nu$. The value of n is $1/2$ for allowed transition. Plots of $(\alpha h\nu)^2$ against $h\nu$ for CuSe prepared at different temperatures are shown in Figure 2.11. The values of the optical energy gap were determined by extrapolating the linear portion of the curves. The band gap for the samples is listed in Table 2.1. From this table, we notice that, the optical band gap decreases from 1.41 to 1.37 eV. This means that, the optical band gap decreases with increasing temperature which is due to the quantum size effect (Seoudi *et al.*, 2006). The absorbance of the sample is given by $A = -\log_e \exp(-\alpha \Delta t)$ and thus $\alpha = A/\Delta t$. The absorption coefficient is related to the photon energy by:

$$\alpha = \alpha_o (h\nu - E_g)^n$$

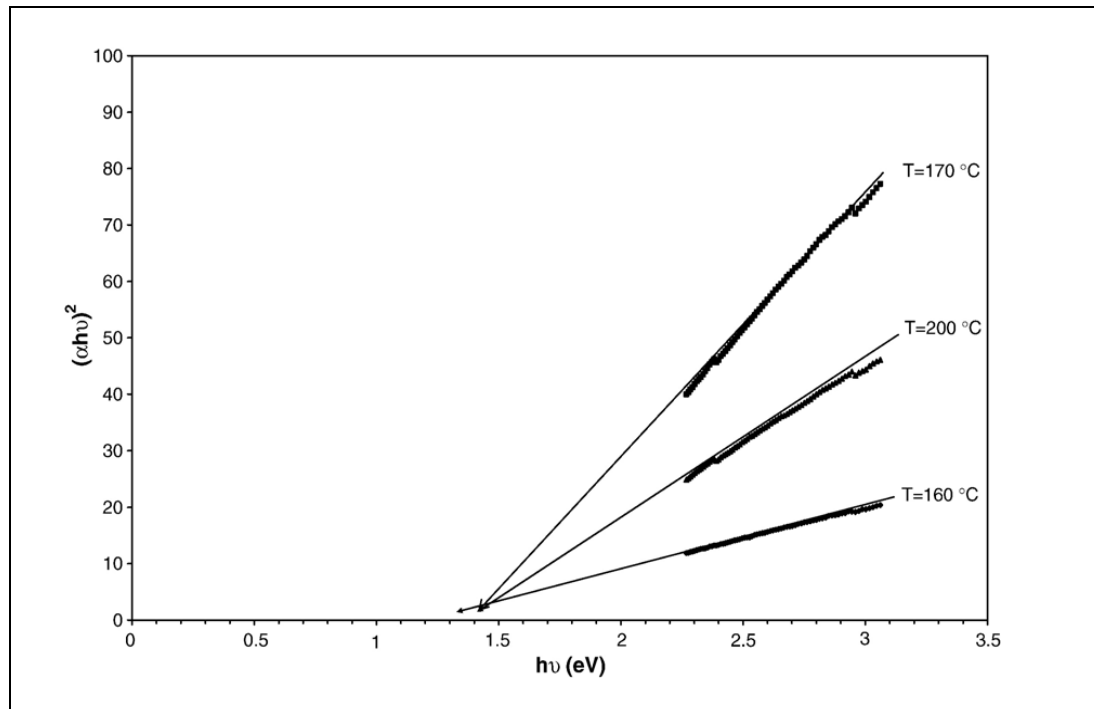


Figure 2.11: Relation between $(\alpha h\nu)^2$ and photon energy ($h\nu$) for CuSe prepared at $T=160$ °C, 170 °C and $T=200$ °C (Seoudi *et al.*, 2006).

Table 2.1: The optical band gap was measured at room temperature for CuSe nanocrystalline prepared at 160, 170 and 200 °C

Temperature (°C)	Optical band gap E_g (eV)
160	1.41
170	1.40
200	1.37

2.10 Photon absorption in a direct and indirect band gap semiconductor

The energy gap (E_g) is a feature of semiconductors which determines their applications in optoelectronics. Due to low scattering in solid films, it is easy to extract the E_g values from their absorption spectra knowing their thickness. However, in colloidal samples, the scattering effect is enhanced since more superficial area is exposed to the light beam (Sakr *et al.*, 2010). The band structure plays crucial role in light absorption and emission of a semiconductor.

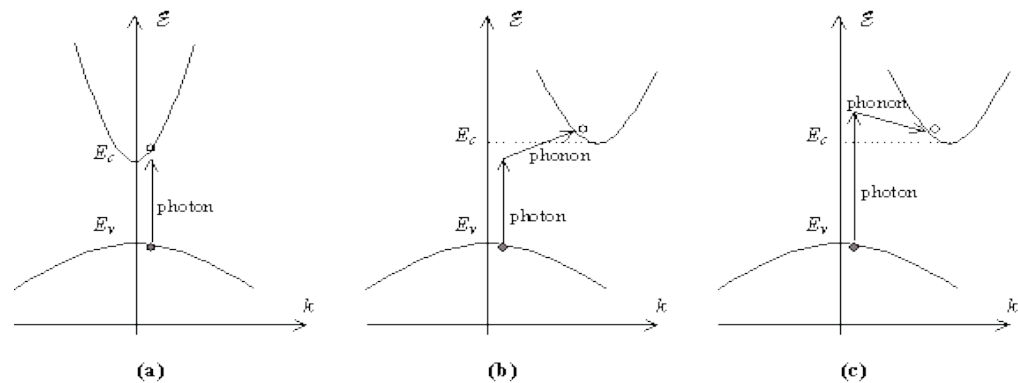


Figure 2.12: E - k diagram illustrating a) Photon absorption in a direct band gap semiconductor b) Photon absorption in an indirect band gap semiconductor assisted by phonon absorption and c) Photon absorption in an indirect band gap semiconductor assisted by phonon emission. (adapted from : http://ecee.colorado.edu/~bart/book/book/chapter4/ch4_6.htm)

CHAPTER 3

Methods

3.1 Chemical used

Table 3.1: Chemical used to synthesis Copper selenide (CuSe) nanoparticles

Chemical	Molecular Formula	Manufacturer
N-Cetyl-N,N,N-trimethylammonium Bromide	$C_{19}H_{42}BrN$	R&M chemicals (99.00%)
Cyclohexane	C_6H_{12}	Sigma-Aldrich (99.00%)
Copper(II) chloride dehydrate	$CuCl_2 \cdot 2H_2O$	R & M chemicals (99.00%)
Sodium selenite	Na_2SeO_3	Sigma-Aldrich (99.00%)
Sodium borohydride	$NaBH_4$	ACROS Organic (98.00%)
Absolute ethanol	C_2H_5OH	Gene Chemical (99.70%)
Toluene	$C_6H_5CH_3$	J.T. Baker (67.00%)

3.2 Apparatus

250 ml conical flask and 50 ml beaker, droppers, hot plate, magnetic stirrer and magnetic bar, centrifuge tube, spatula, micro-spatula, sample bottles

3.3 Synthesis of Copper Selenide using Ternary Water-in-oil emulsion System

3.3.1 Effect of reducing Agent Concentration

The volume ratio of DI water and cyclohexane was maintained at 2:1. 10 ml of deionised water and 5 ml of cyclohexane was added into a beaker followed by 0.1 M CTAB. The mixture was stirred until homogeneous mixture achieved. 10 ml of $\text{CuCl}_2 \cdot 2\text{H}_2\text{O}$ (0.1 M) reactant was prepared. Then, 10 ml of second reactant, Na_2SeO_3 (0.1M) was added into a new beaker followed by 5 ml of sodium borohydride which is changed accordingly. This second reactant mixture was stirred for 30 minutes. The copper chloride that solubilised in DI water was added into the emulsion system followed by the second reactant mixture directly to the system. The solution becomes dark brown after the addition of the second reactant. The mixture was stirred for 1 hour. Preparation of the sample at various concentration of reducing agent was summarised in the Table 3.2 and Figure 3.1.

Table 3.2: Preparation of sample at various concentrations of reducing agent (NaBH₄)

Sample	DI H ₂ O (mL)	Cyclohexane (mL)	CTAB		Cu ²⁺			Se ²⁻			Time of stirring	Autoclave	Conc. Of NaBH ₄ (mol dm ⁻³)
			Conc. (mol dm ⁻³)	Mole	Conc. (mol dm ⁻³)	Vol. of DI to dissolve (mL)	Mole	Conc. (mol dm ⁻³)	Vol. of DI to dissolve (mL)	Mole			
S3020	10	5	0.1	0.001	0.1	50	0.005	0.1	50	0.005	1h	30 mins, 121 ^o c	2.0
S3025	10	5	0.1	0.001	0.1	50	0.005	0.1	50	0.005	1h	30 mins, 121 ^o c	2.5
S3030	10	5	0.1	0.001	0.1	50	0.005	0.1	50	0.005	1h	30 mins, 121 ^o c	3.0

(Note: The step calculation of mole and concentration for each reactant were shown in Appendix A)

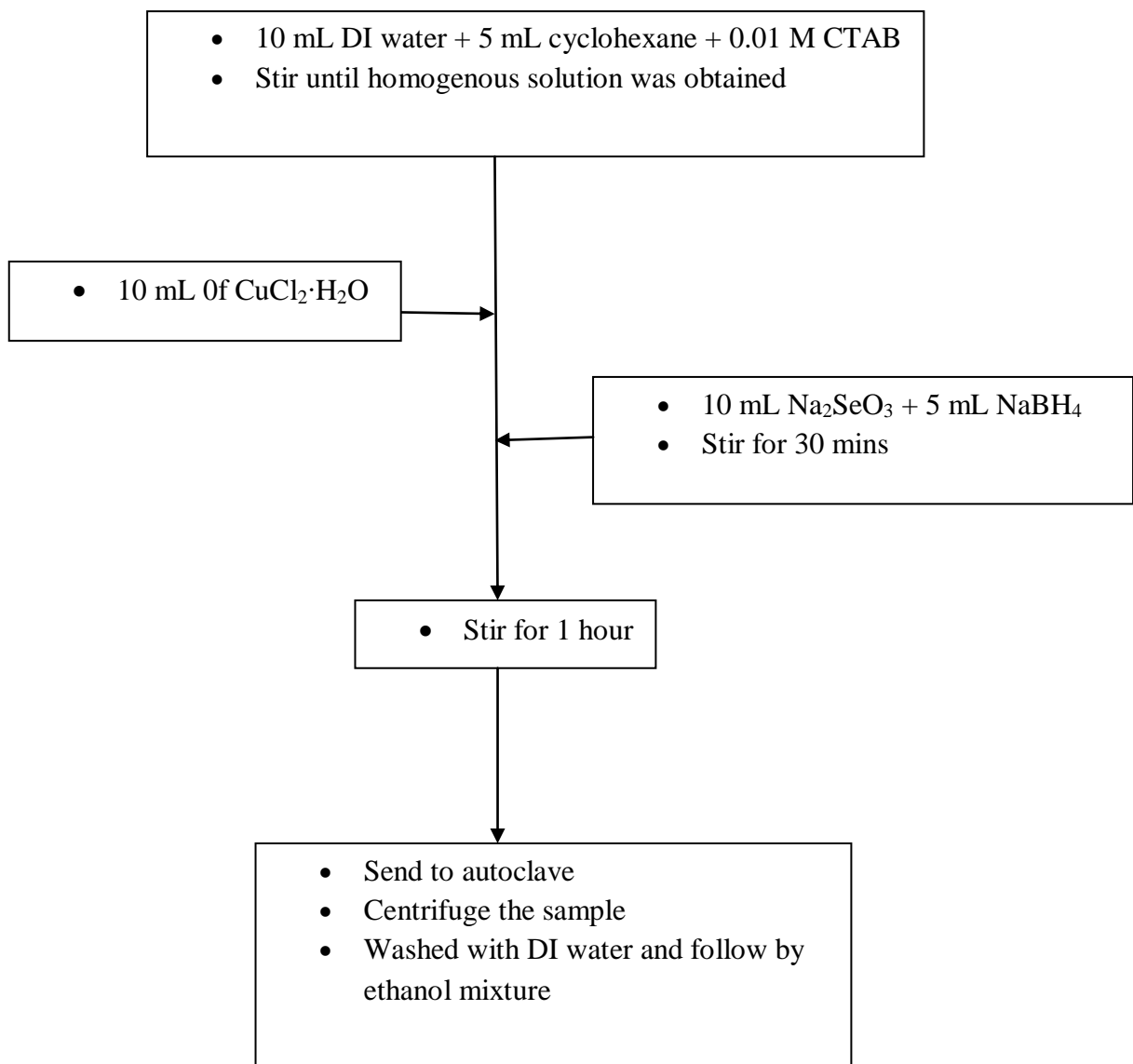


Figure 3.1: Flowchart of synthesising CuSe at various concentration of reducing agent, NaBH₄

3.3.2 Effect of stirring

The volume ratio of DI water and cyclohexane was maintained at 2:1. 10 mL of deionised water and 5 mL of cyclohexane was added into a beaker followed by 0.1 M CTAB. The mixture was stirred for until homogenous. 10 mL of $\text{CuCl}_2 \cdot \text{H}_2\text{O}$ (0.1 M) was added into it with continuously stirring. Then 10 mL Na_2SeO_3 (0.1 M) was reduced by adding 5 mL of sodium borohydride (2.0 M). This second reactant mixture was stirred for 30 minutes. The copper chloride that solubilised inside DI water was added into the emulsion system followed by the second reactant mixture directly to the system. The mixture was stirred at different time of stirring as summarised in Table 3.3. The CuSe precipitate was in dark-brown in colour.

Table 3.3: Preparation of CuSe sample at different period (time of stirring)

Sample code	$\text{CuCl}_2 \cdot \text{H}_2\text{O}$ (mol/dm ³)	Na_2SeO_3 (mol/dm ³)	NaBH_4 (mol/dm ³)	Time of stirring (hour)
S30201	0.10	0.10	2.0	1
S30202	0.10	0.10	2.0	2
S30203	0.10	0.10	2.0	3

(Note: The step calculation of mole and concentration for each reactant were shown in Appendix A)

3.3.3 Effect of autoclaved period

The volume ratio of DI water and cyclohexane was maintained at 2:1. 10 mL of deionised water and 5 mL of cyclohexane was added into a beaker followed by 0.1 M CTAB. The mixture was stirred until homogeneous mixture. Then, 10 mL of $\text{CuCl}_2 \cdot \text{H}_2\text{O}$ (0.1 M) was added into it. Meanwhile, 10 mL Na_2SeO_3 (0.1 M) was reduced by adding 5 mL of sodium borohydride (2.0M) which was stirred about 30 minutes. The copper chloride that solubilised in DI water was added into the emulsion system followed by the second reactant mixture directly to the system. The mixture was stirred for 1 hour and then taking to heat-treatment at various periods which was summarised in Table 3.4.

Table 3.4: Preparation of CuSe sample at various heated-treatment periods

Sample code	$\text{CuCl}_2 \cdot \text{H}_2\text{O}$ (mol/dm ³)	Na_2SeO_3 (mol/dm ³)	NaBH_4 (mol/dm ³)	Time of stirring (hour)	Time of autoclave period (minute)
S3020	0.10	0.10	2.0	1	30
S30202	0.10	0.10	2.0	1	60
S30203	0.10	0.10	2.0	1	90

(Note: The step calculation of mole and concentration for each reactant were shown in Appendix A)

3.3.4 Centrifugation of samples



Figure 3.2: Centrifugation instrument model Sigma Sartorius 2-1

Figure 3.2 shows centrifuge instrument used to carry out centrifugation of CuSe. The centrifugation is a process used to isolate or concentrate fine materials that finely dispersed in the solution. It is used is based on the principle of gravity effect the particle suspended. In general, the nano-sized particles suspended in the sample will be isolated from the liquid phase in a centrifuge tube was spun in the specific holes of the rotor and the rotation speed of the rotation was measured in revolution per minute (rpm). The rotor is made by dense metal which dissipates heat quickly and sufficient mass to generate momentum. The process work under vacuum condition and refrigerated to reduce heating caused by frictional forces as the rotor spins by stored the rotor in refrigeration units which keep them near the operating temperature.

This process was carried out for all the samples that prepared at different parameters as summarised in Table 3.2, Table 3.3 and Table 3.4. The deposited precipitates with the solution mixture were transferred into centrifuge tube to be isolated from the emulsions system by using centrifugation. The centrifugation process was performed at 6000 rpm for 3 minutes. After centrifugation, the solution was disposed slowly to avoid loss of product and the precipitates obtain at the bottom of the centrifuge tube was washed with the deionised water for the next run. The sample was washed with DI water until clear solution obtains at the top of the centrifuge tube. Then, the washing process was continuing with the volume ratio of ethanol: water mixture (1:1) until no more emulsion in the product. The sample was washed with DI water to avoid the presence of any impurities and with ethanol: water mixture to remove unreacted ions and to destabilise the emulsion so that the precipitates can be isolated. The precipitate was dried in the oven at 50°C for overnight. Finally, the sample was transferred into labelled sample vial and stored in the dry box.

3.4 Characterisations

The samples property evaluation were characterised by using Shimadzu X-ray Diffractometer LabX XRD-6000 as shown in Figure 3.3 and UV-Vis absorption spectra were recorded on a Perkin Elmer Lambda 35 spectrophotometer as shown in Figure 3.6 as well as Fluorescence Spectrophotometer, Perkin Elmer Precisely LS 55 as shown in Figure 3.8.

3.4.1 X-ray Diffraction (XRD)



Figure 3.3: Shimadzu X-ray Diffractometer (LabX XRD-6000)

X-ray diffractometer is used as a fingerprint method for detecting the presence of a known compound or phase in a product. There are over 150,000 unique powder diffraction patterns have been collected from organic, organometallic, inorganic and mineral samples. These have been compiled into a database known as the JCPDS (Joint Committee on Powder Diffraction Standards) files (Dann, 2002).

X-ray powder diffraction (XRD) provides information on unit cell dimensions as it is an analytical technique used for phase identification of a crystalline material. The analysed material is finely ground, homogenised, and average bulk composition is determined.

A large number randomly oriented small crystals also known as crystallites are contained in finely ground crystalline powdered sample (Dann 2002). Each small crystals in the powder will show different crystallites sizes which make up by their based structure of interplanar of atom or ion arrangements, known as crystal plane which are described in Miller indices. Diffraction occurred by diffracted the incident beam to make a 2θ and angle with the planes of the crystallites toward the diffracted beam when a monochromatic X-ray beam shoots on a sample. This angle is called Bragg angle. The model of crystalline structure study of solid using X-rays is shown in Figure 3.4.

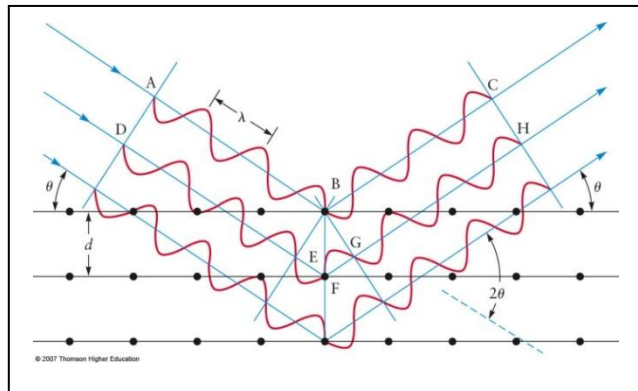


Figure 3.4: Diagram for Bragg reflection from a set of crystal planes with a spacing of d . (adapted from Housecroft and Sharpe, 2008)

In the modern diffraction method, collection of powder diffraction patterns is now almost performed by diffractometers as shown in the schematic diagram of Figure 3.5. Theoretically, the X-rays photons are focused through a slit onto the sample and scattered in all directions. Thus, by the movement of the detector around the sample along the circumference of a circle, it enables the collection of all the reflections corresponding to various hkl (Hammond, 2009).

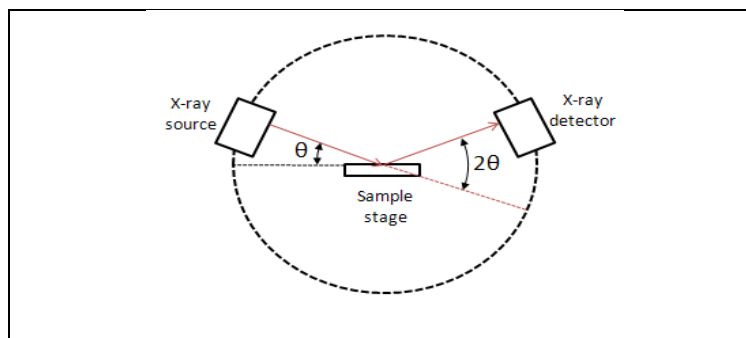


Figure 3.5: A schematic diagram of a powder diffractometer (adapted from: http://chemwiki.ucdavis.edu/analytical_chemistry/instrumental_analysis/powder_x-ray_diffraction)

A convergent beam strikes the sample and the intensity as a function of diffraction angle, 2θ is measured. The width generated in a peak which known as full width at half maximum (FWHM) can be used to calculate the mean crystallites sizes at the planes by using Debye-Scherrer equation. As the crystallite size decreases, the width of the diffraction pattern increases (Smart and Moore, 2005). The Debye-Scherrer formula was shown as below:

$$D = \frac{k\lambda}{B \cos\theta}$$

where D is the crystallite thickness,

λ is the wavelength of the X-rays,

θ is the Bragg angle,

B is the FWHM of the peak corrected for instrumental broadening

The X-ray diffraction patterns of samples were obtained by using parameters of operating at 40 kV and 30 mA, Cu k_{α} radiation and $\lambda = 1.5419 \text{ \AA}$, scanning speed 1.00 degree/min and the 2θ scan range from 20 to 60°.

3.4.2 Optical Properties

UV/Vis Spectrophotometer used to run absorption test on the sample CuSe nanoparticles is Perkin Elmer Lambda 35 UV/Vis Spectrophotometer which was shown as below Figure 3.6



Figure 3.6: Perkin Elmer Lambda 35 UV/Vis Spectrophotometer

The UV/Vis spectrometer used for the research is a double beam spectrometer. Figure 3.6 shows the diagram of double beam UV/Vis spectrometer. The UV-Vis absorption spectroscopy is frequently used to characterise semiconductors thin films and to determine the band gap of the nanostructure CuSe and also to understand the quantum confinement of the CuSe. The most dramatic property of semiconductor nanoparticles is the size evolution of the optical absorption spectra. Hence UV-visible absorption spectroscopy is an efficient technique to monitor the optical properties of quantum-sized particles (Pradeep, 2008). Figure 3.7 shows that diagram of double beam UV/Vis spectrometer.

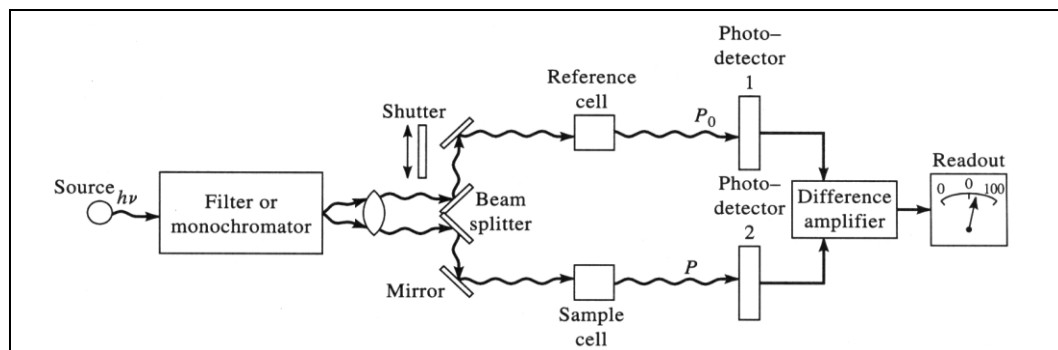


Figure 3.7: Diagram of double beam UV/Vis spectrometer. (adapted from: http://www.chemistry.mtu.edu/~hyliu/ch4212/Powerpoint/An_introduction_%20to_ultraviolet_Visible.pdf)

UV-vis spectroscopy involves photons in UV-visible region. This means it uses light in the visible and adjacent near ultraviolet (UV) and near infrared (NIR)-ranges (Rouessac, 1994). The absorption in the visible ranges directly affects the colour of the chemicals involved. In this region of the electromagnetic spectrum, molecules undergo electronic transitions. Generally, wavelength of the maximum excitation absorption decreases as particle size decreases.

UV-Vis absorption spectroscopy is carried out dispersing the sample in liquid media like ethanol. The nanoparticles were redispersed by the sonication bath in order to obtain better particle dispersion (Khiew *et al.*, 2003). If the particle size of the sample is not small enough, it precipitates and the absorption spectrum is even more difficult to interpret. (Sakr *et al.*, 2010). Quartz cuvette was used to run the test as Quartz (silica) which is used for the UV region because it is transparent below 350 nm. The UV-Vis absorption spectra of the solutions were recorded on a Perkin-Elmer Lambda 35 Spectrophotometer in the wavelength range 200-800 nm.

3.4.3 Photoluminescence (PL) Spectrophotometer



Figure 3.8: Fluorescence Spectrophotometer, Perkin Elmer Precisely LS 55

The characterisation of photoluminescence property of CuSe was done by using Perkin Elmer LS 55 Fluorescence Spectrometer. Fluorescence spectrophotometer is an instrument that used to test the photoluminescence (PL) of a compound. The PL is an important technique used to measure the purity and optical properties of semiconductors.

PL is a process where an absorbed photon (electromagnetic radiation) at higher level energy states in a substance after excitation returned back to the lower energy state by releasing a photon. Electron de-excitation occurs almost spontaneously and in which emission from a luminescent substance stops when the exciting source is removed. As a molecule is excited to an electronic state of E_1 from its ground state, E_0 , the excess energy is removed through fluorescence emission. Fluorescence occurs from the lowest vibrational level of E_1 to various vibrational levels of E_0 and at a longer wavelength than the radiation that caused the excitation which has shown in Figure 3.9.

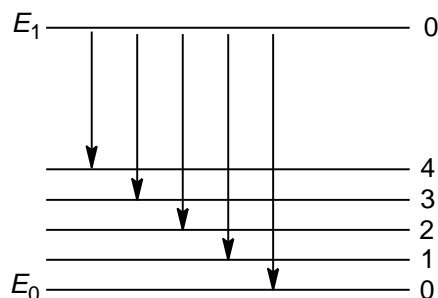


Figure 3.9: Energy level diagram of fluorescence occurrence. (adapted from: <http://web.njit.edu/~gary/321/Lecture5.html>)

As in my research, the sample to be analysed must do some preparations to obtain a well disperse CuSe solution due to the nanoparticles easily settled down. Therefore, a very little powder was transferred into a sample vial since the fluorescence spectrophotometer is very sensitive to concentration and any overshoot peaks will not be able to interpret. Then, a few drops of toluene were poured inside the sample vial and these steps were repeated for the following samples. After this, the sample vial was ultrasonicated in a sonicator to finely disperse the nanoparticles. Finally, the solution was transferred into a Quartz cell cuvette and placed it into fluorescence spectrophotometer analysis. Unlike UV-Vis Spectrophotometer, this spectrophotometer does not require the use of reference cell. The sample was placed in the quartz cell, where it should not exceed the three quarter level of the cell. The photoluminescence analysis of CuSe in toluene solution were carried out under the following parameters whereby, Xe lamp was used, both excitations and emission slits were set at 15 nm, scan speed 500 nm/min and the excitation wavelength was varied from 200 to 300 nm, 10 nm intervals at 27°C.

CHAPTER 4

RESULTS AND DISCUSSION

4.1 Results

In this experiment, the formation of micelles system is involved in the synthesis of copper selenide nanoparticles. Upon mixing all of the solution, a dark brown colour solution appeared which indicates that the presence of selenide source have been reduced to Se^{2-} . The solution contains the surfactant molecules, CTAB, acting as the stabiliser for the emulsion system. During the reaction, the mixture was stirred vigorously by using hot-plate to ensure a completed reaction and to stabilise the emulsion system. With stirring, the stability of the emulsion system can be maintained and agglomeration of particles can be prevented.

The surfactant employed in this experiment is CTAB, a cationic surfactant whose hydrophilic headgroup carries a net positive charge. The presence of surfactant will affect the growth and particles characteristics significantly. It is very important in the particle formation due to its ability for compartmentalisation. The positively charged headgroups can easily attach the metal clusters' surface to make them soluble in the water environment; the cetyl hydrophobic chain is toward to oil phase.

Apart from surfactant, another material used in this synthesis is sodium borohydride, NaBH_4 . It is a strong soluble hydride reducing agent, and is capable in reducing the Na_2SeO_3 source to Se^{2-} . The reducing agent was added to the solution under stirring condition about 30 minutes. The formation of micelle system in synthesis of copper selenide nanoparticles is illustrated in Figure 4.1.

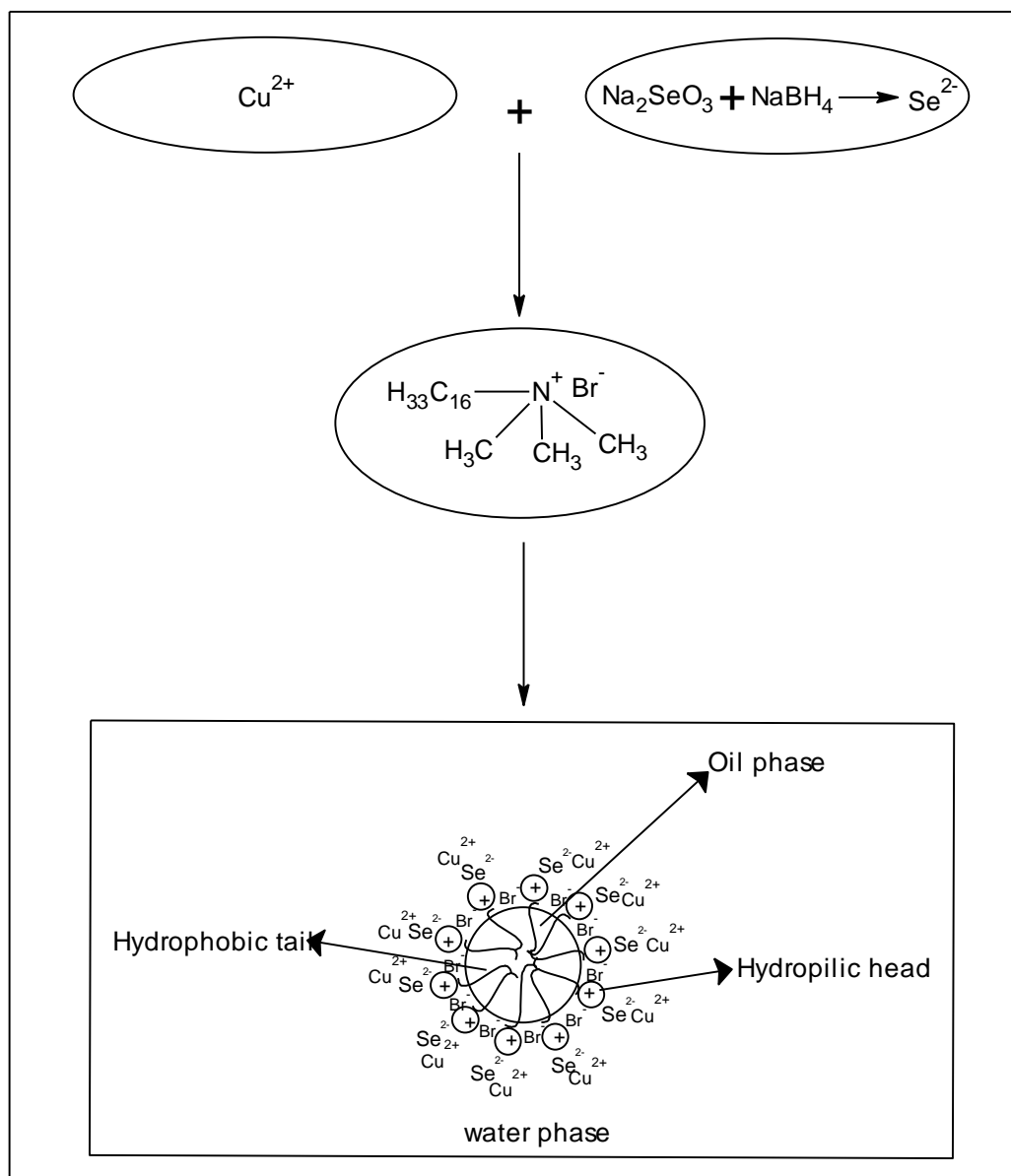


Figure 4.1: Formation of micelle system in synthesis of copper selenide nanoparticles.

In this research, the samples of copper selenide nanoparticles synthesised in different parameters were characterised by using X-ray Diffractometer, UV-Vis (UV-Vis) Spectrophotometer and Photoluminescence (PL) Spectrophotometer. These characterisations were carried out under room temperature condition.

4.1.1 X-Ray Diffractometer (XRD)

The seven samples synthesised in different parameters of various concentrations of reducing agent, $[\text{NaBH}_4]$, effect of stirring period and effect of autoclave period were characterised by using X-ray Diffractometer and the results obtained are shown in Figure 4.2 - 4.4, respectively. Meanwhile, the matching of the 2θ and d -spacing values for each peaks of the samples with JCPDS No. 00-020-1020 corresponding to the hexagonal phase CuSe. The summaries of these matching of the 2θ and d -spacing values for each peaks of the sample are shown in Table 4.1 - 4.3, respectively.

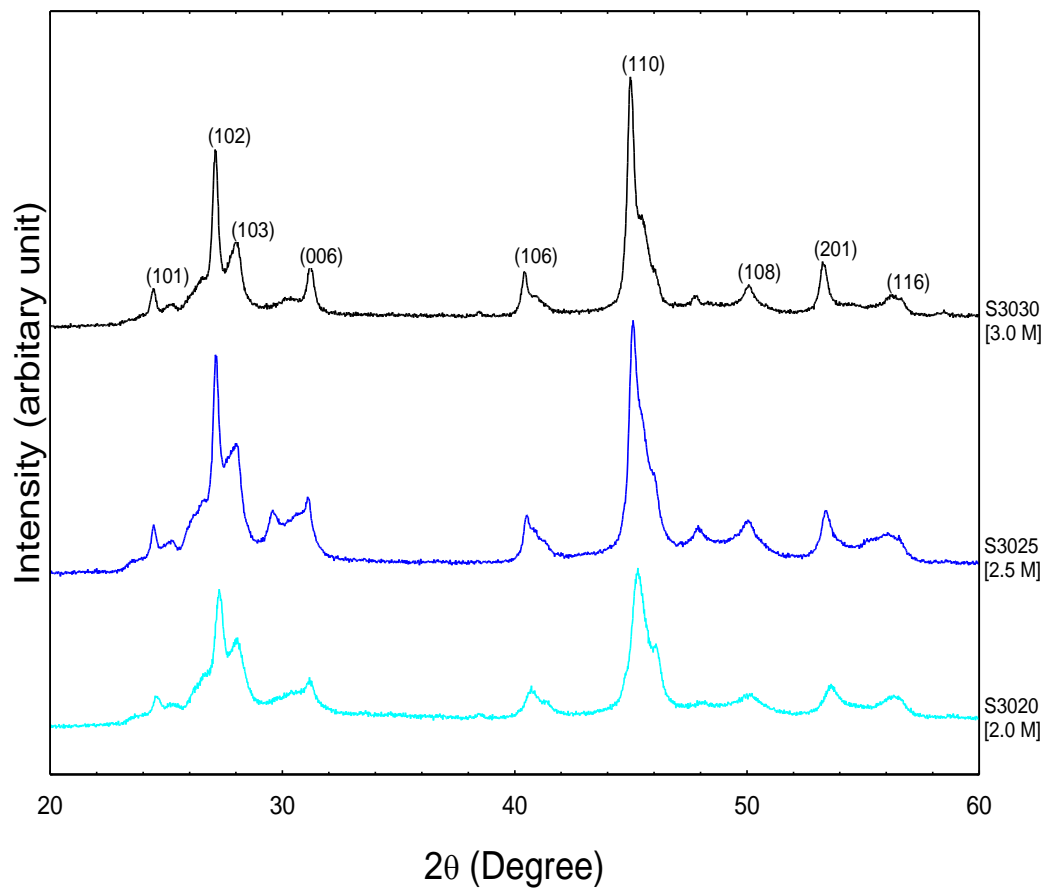


Figure 4.2: XRD pattern of samples prepared at various reducing agent concentration, $[\text{NaBH}_4]$

Table 4.1: XRD data for sample prepared at various reducing agent concentration

Sample Code	2θ (°)	<i>d</i> -spacing (Å)	2θ (°)	<i>d</i> -spacing (Å)	2θ (°)	<i>d</i> -spacing (Å)	2θ (°)	<i>d</i> -spacing (Å)	2θ (°)	<i>d</i> -spacing (Å)	2θ (°)	<i>d</i> -spacing (Å)	2θ (°)	<i>d</i> -spacing (Å)
JCPDS No. 00-020-1020	46.08	1.968	31.14	2.870	28.12	3.170	30.49	2.929	40.93	2.203	50.08	1.820	54.09	1.694
S3020	45.43	1.995	31.10	2.873	27.98	3.186	30.04	2.972	40.86	2.206	49.86	1.828	53.65	1.707
S3025	45.26	2.002	30.98	2.884	27.88	3.198	30.98	2.884	40.71	2.215	48.86	1.828	53.41	1.714
S3030	44.97	2.014	31.18	2.866	27.96	3.188	30.20	2.957	40.96	2.201	50.04	1.821	53.26	1.718
(<i>hkl</i>)	110		006		102		103		106		108		201	
Unit cell	Hexagonal													

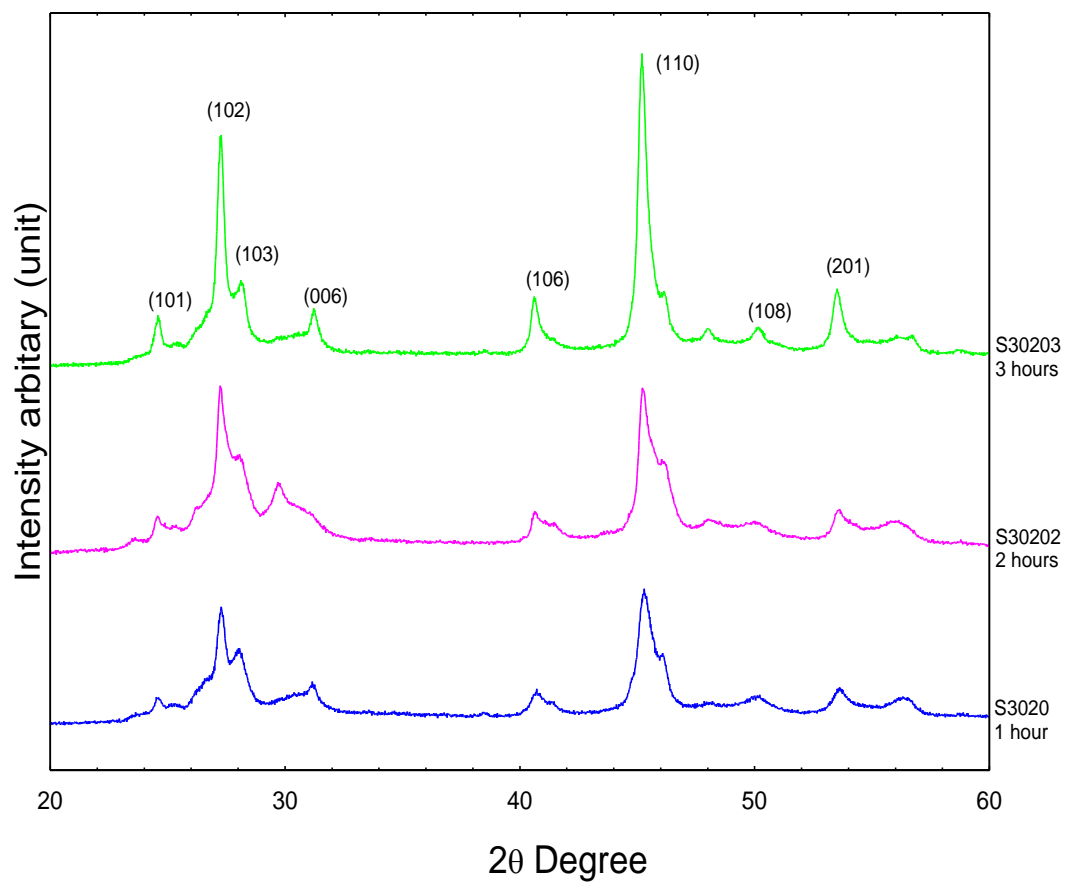
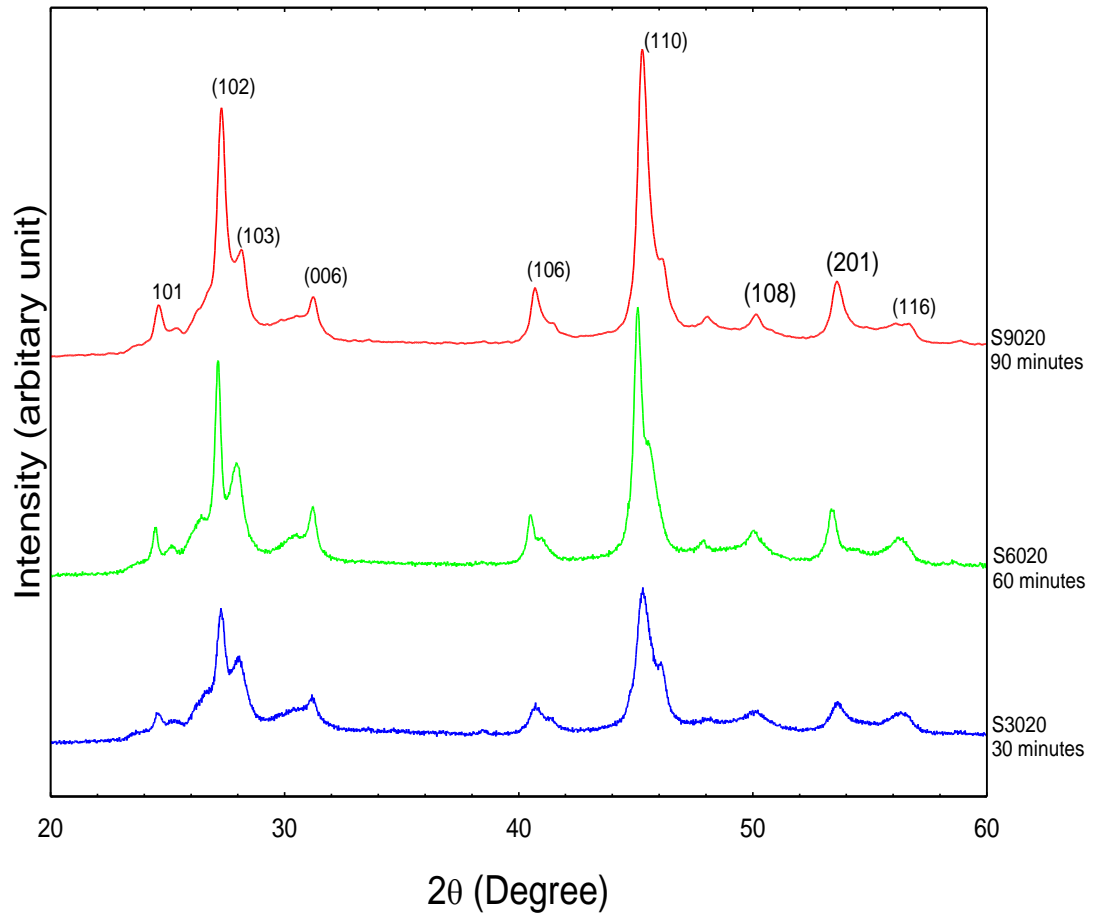


Figure 4.3: XRD pattern of samples prepared at various periods (under stirring condition)

Table 4.2: XRD data for sample prepared at various stirring period

Sample Code	2 θ (°)	<i>d</i> -spacing (Å)	2 θ (°)	<i>d</i> -spacing (Å)	2 θ (°)	<i>d</i> -spacing (Å)	2 θ (°)	<i>d</i> -spacing (Å)	2 θ (°)	<i>d</i> -spacing (Å)	2 θ (°)	<i>d</i> -spacing (Å)	2 θ (°)	<i>d</i> -spacing (Å)
JCPDS No. 00-020-1020	46.08	1.968	31.14	2.870	28.12	3.170	30.49	2.929	40.93	2.203	50.08	1.820	54.09	1.694
S3020	45.43	1.995	31.10	2.873	27.98	3.186	30.04	2.972	40.86	2.206	49.86	1.828	53.65	1.707
S30202	45.49	1.992	31.20	2.864	28.00	3.184	30.40	2.938	40.91	2.204	50.08	1.820	53.63	1.708
S30203	45.20	2.004	31.18	2.866	28.08	3.175	30.44	2.934	40.62	2.219	50.09	1.820	53.49	1.712
(<i>hkl</i>)	110		006		102		103		106		108		201	
Unit cell	Hexagonal													



**Figure 4.4: XRD pattern of samples prepared at various periods
(under autoclave condition)**

Table 4.3: XRD data for sample prepared at various heated-treatment period

Sample Code	2 θ (°)	<i>d</i> -spacing (Å)	2 θ (°)	<i>d</i> -spacing (Å)	2 θ (°)	<i>d</i> -spacing (Å)	2 θ (°)	<i>d</i> -spacing (Å)	2 θ (°)	<i>d</i> -spacing (Å)	2 θ (°)	<i>d</i> -spacing (Å)	2 θ (°)	<i>d</i> -spacing (Å)
JCPDS No. 00-020-1020	46.08	1.968	31.14	2.870	28.12	3.170	30.49	2.929	40.93	2.203	50.08	1.820	54.09	1.694
S3020	45.43	1.995	31.10	2.873	27.98	3.186	30.04	2.972	40.86	2.206	49.86	1.828	53.65	1.707
S9020	45.21	2.004	31.16	2.868	27.14	3.283	30.42	2.936	40.66	2.217	49.95	1.824	53.36	1.716
S6020	45.30	2.000	31.20	2.864	27.29	3.265	30.54	2.925	40.72	2.214	50.07	1.820	53.60	1.709
(<i>hkl</i>)	110		006		102		103		106		108		201	
Unit cell	Hexagonal													

X-Ray diffraction is the principal method used to identify the phase present in solid-state material. According to the crystallite size that is performed by measuring the broadening of a particular XRD peaks in a diffraction pattern associated with a particular planar reflection from within the crystal unit cell. Thus, if the full width at half maximum (FWHM) of the diffraction angle is given, the mean crystallite sizes of the samples can be calculated through Debye-Scherrer's equation which is shown as below:

$$D = \frac{k \lambda}{\beta \cos\theta}$$

Where, D = mean crystallite size perpendicular to normal line of (hkl) plane

K = constant equal to 0.9

λ = the X-Ray wavelength, 1.5419 Å

β = FWHM of the (hkl) diffraction peak in radian

θ = Bragg angle of the (hkl) diffraction peak

By using Debye-Scherrer's equation, the main XRD peaks of plane (110) were chosen to calculate the mean crystallite size in order to minimise errors. The mean crystallite size calculated for the selected samples were shown in Table 4.4.

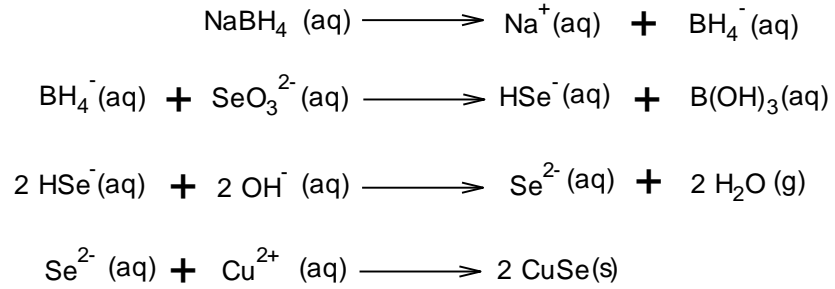
Table 4.4: Comparison of mean crystallite size for seven samples

Sample code	FWHM in 2θ ($^{\circ}$)	β calculated from FWHM in radian	2θ of (110) peak ($^{\circ}$)	θ of (110) peak ($^{\circ}$)	Calculated mean crystallite size (nm)
S3020	1.0709	0.0187	45.4245	22.7123	8.0447
S3025	0.9943	0.0174	45.2582	22.6291	8.6405
S3030	0.4236	0.0074	44.9708	22.4854	20.2958
S6020	0.8855	0.0155	45.2062	22.6031	9.6979
S9020	0.6247	0.0109	45.3018	22.6509	13.7953
S30202	1.2762	0.0223	45.4928	22.7464	6.7477
S30203	0.5580	0.0097	45.2033	22.6017	15.4964

(Note: The calculation and graph of comparison between mean crystallite size versus each parameter used are shown in Appendix B)

The XRD patterns for all the CuSe samples of are shown in Figure 4.2 - 4.4, respectively. From the three Figures which show that there are nine peaks appeared in the spectrum. The 2θ and d -spacing values of these peaks given by the diffraction patterns were matched with the standard database values of JCPDS card No. 00-020-1020 which has been summarised in Table 4.1 - 4.3, respectively. From these Figures, the diffraction patterns of three predominant peaks were exhibited at about 46.00, 31.00 and 28.00 degrees, which were indexed to scattering from the (110), (006) and (102) planes of hexagonal phase CuSe. Therefore, the hexagonal phase CuSe had been considered successfully synthesised by adding reducing agent, increasing period of stirring and heated-treatment.

The reducing agent, NaBH₄ was introduced in synthesising of copper selenide nanoparticles. It will reduce the selenite ions (SeO₃²⁻) to selenide ions (Se²⁻). The chemical reaction can be formulated as follows:



(Ambade *et al.*, 2006)

From the above reaction equation, it shows that sodium selenite, Na₂SeO₃ released higher concentration of Se²⁻ in the presence of reducing agent. Then, Se²⁻ source only can react with the Cu²⁺ solution to form CuSe nanostructure. In addition, the mean crystallite size was increased by increasing the reducing agent as this will facilitate the growth of nanoparticles under non-equilibrium kinetic growth conditions. To conclude, NaBH₄ favors the formation of copper selenide nanostructure.

Figure 4.3 shows XRD pattern of samples prepared at various periods under stirring condition. The spectrum shows that the peaks were observed to be higher intensity by increasing the period of stirring. Meanwhile, the calculated mean crystallite size was in between 8.0447 – 15.4964 nm while prolonging the period of stirring. This is due to molecules are well mixed which lead to have a

greater chance of colliding, therefore, prolong the stirring period will lead to higher opportunity of collision between the particles and then to form a larger size of the particles. The collision was accelerated under stirring condition.

From Figure 4.4 shows XRD pattern of samples prepared at various heated-treatment periods. The spectrum shows that the peaks were observed to be more intense and narrower by increasing the heated-treatment of reaction time. In addition, the mean crystallite size was increased by increasing the heated-treatment period which is shown in Table 4.4. This is because the reactants can react with each other within a short time. This leads to an increase in the reaction rate and the sizes of the particles increased with increasing in reaction duration, thereby reducing the required reaction durations.

Based on the above observation, one can conclude that small diameter nanoparticles formed at lower concentration of the reducing agent, shorter period of stirring and shorter heated-treatment reaction time. In the meantime, further characterization like transmission electron microscopy (TEM) or scanning electron microscopy (SEM) are needed in order to confirm the size and morphology of the synthesised CuSe.

4.1.2 UV/Vis Spectrophotometer (Optical properties)

All the seven samples synthesised in different parameters were characterised by using UV-Vis Spectrophotometer and the results obtained are shown in Figure 4.5 - 4.7, respectively. Optical properties, which are directly related to the size of nanoparticles, can be studied using the absorption spectra of CuSe.

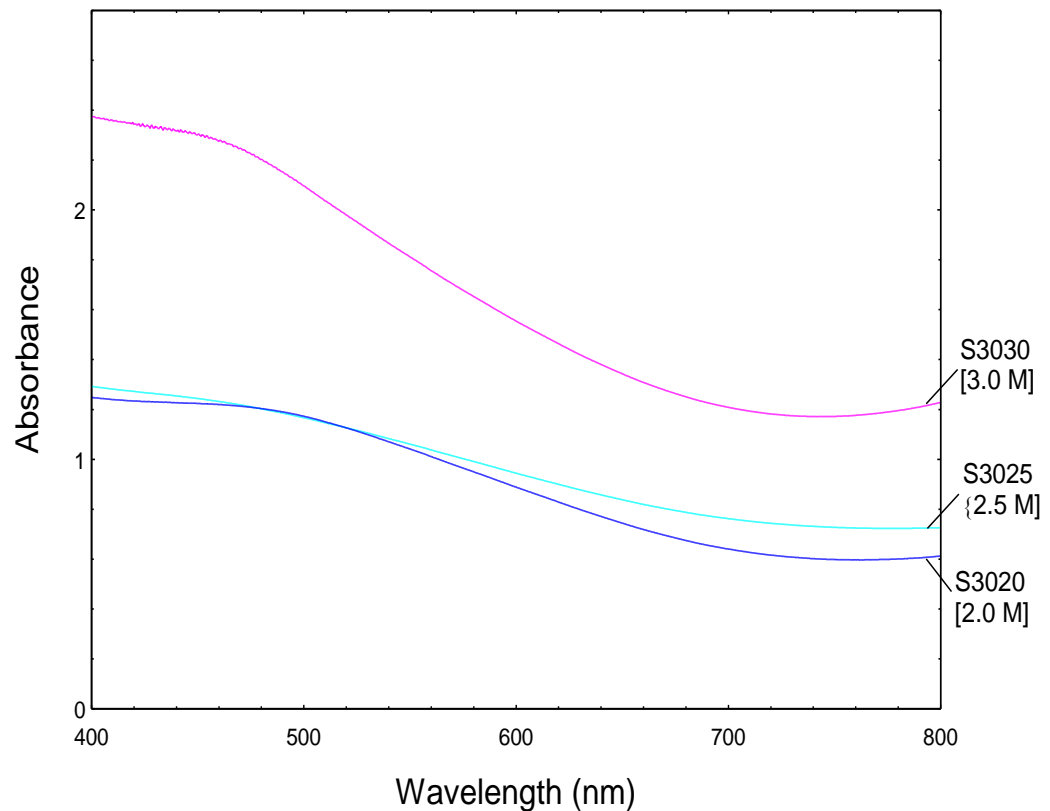


Figure 4.5: UV/Vis absorption spectrum of CuSe nanoparticles at different concentration of reducing agent S3020 = 2.0 M, S3025 = 2.5 M, S3030 = 3.0 M, respectively.

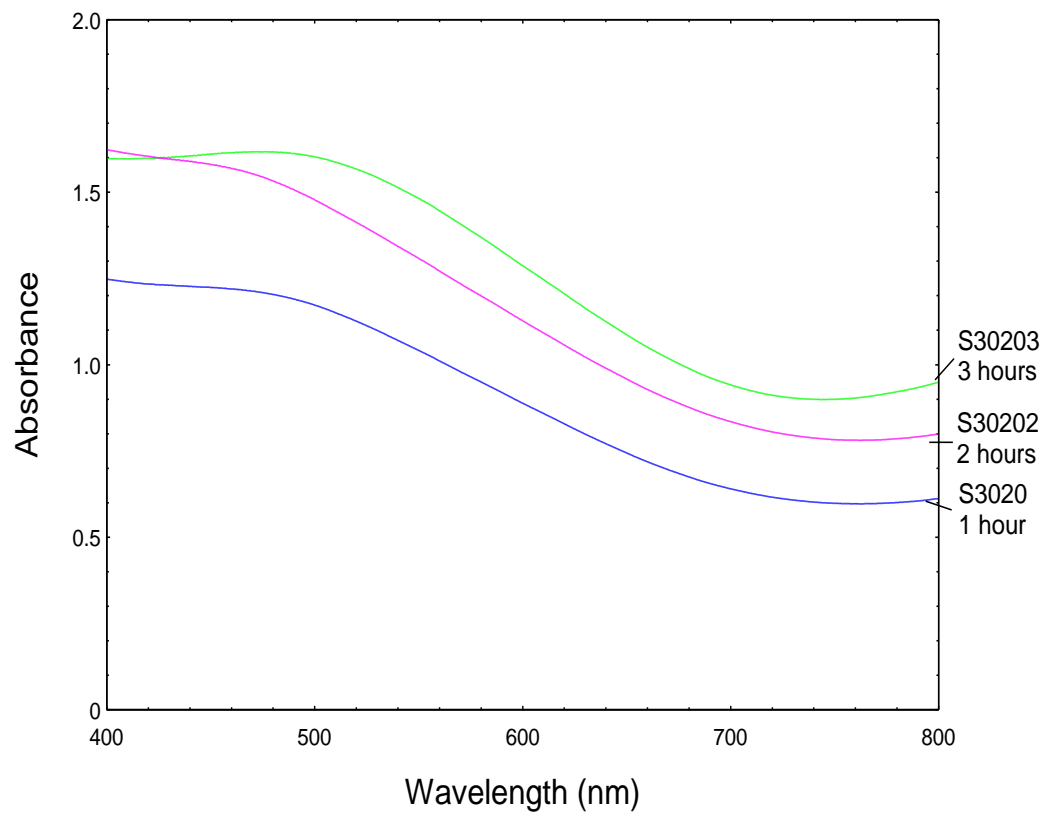


Figure 4.6: UV/Vis absorption of CuSe nanoparticles prepared at different period (under stirring condition) S3020 = 1 hour, S30202 = 2 hours, and S30203 = 3hours, respectively.

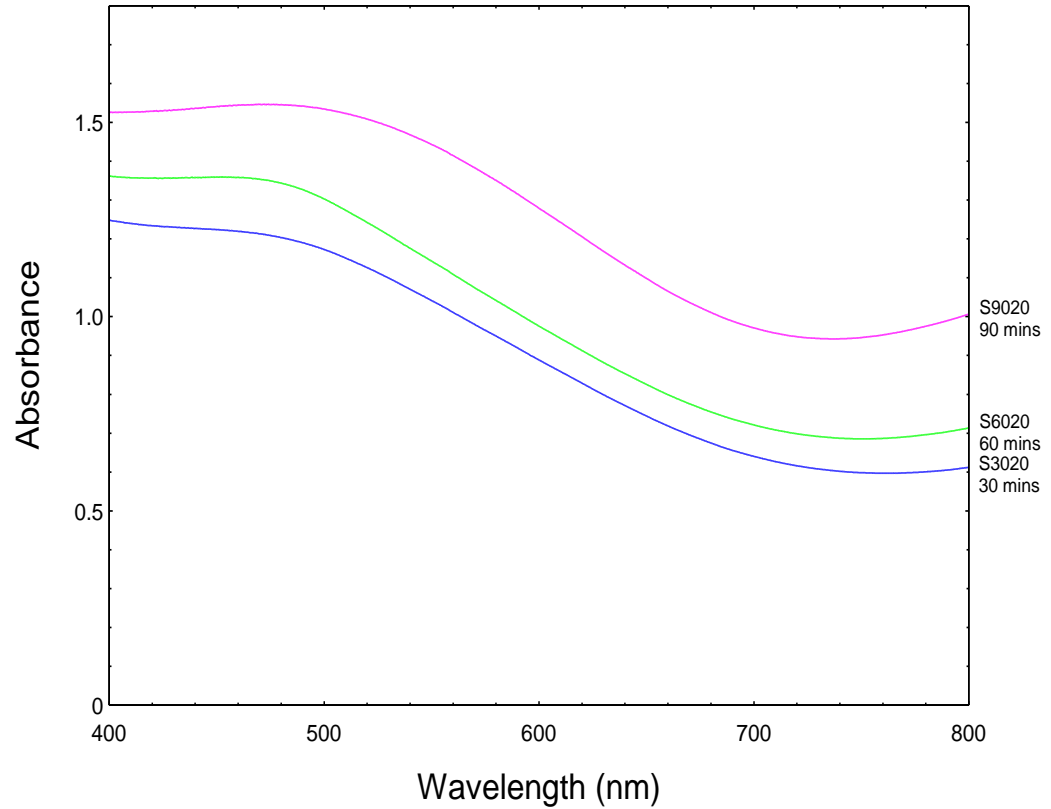


Figure 4.7: UV/Vis absorption of CuSe nanoparticles prepared at different autoclaved period S3020 = 30 minutes, S6020 = 60 minutes, and S9020 = 90 minutes.

Form Figures 4.5 - 4.7 show that the absorption onset wavelength for all the samples approximately 487 nm and they are blue shift. The band gap energy for bulk CuSe is equal to 1.3 eV (Seoudi *et al.*, 2006).

From the figures, it can be observed that the absorption edge move to the blue shift which shift to the shorter wavelength. Therefore, it indicates that decrease in the particle size. This blue shift is due to the quantum confinement effect (Seoudi *et al.*, 2006). It could be concluded that the changes concentration of reducing agent, time of stirring rate and heated-treatment period will have effect on the particle size. This is probably due to the increase of formation rate of nuclei and growth rate of copper selenide nanoparticles. Hence, increasing one of the above effects will lead to the higher nucleation rate of copper selenide nanoparticles formed and growing larger through particle-particle aggregation.

The theory of optical absorption gives the relation between the absorption coefficient and the photon energy, for direct allowed transition as:

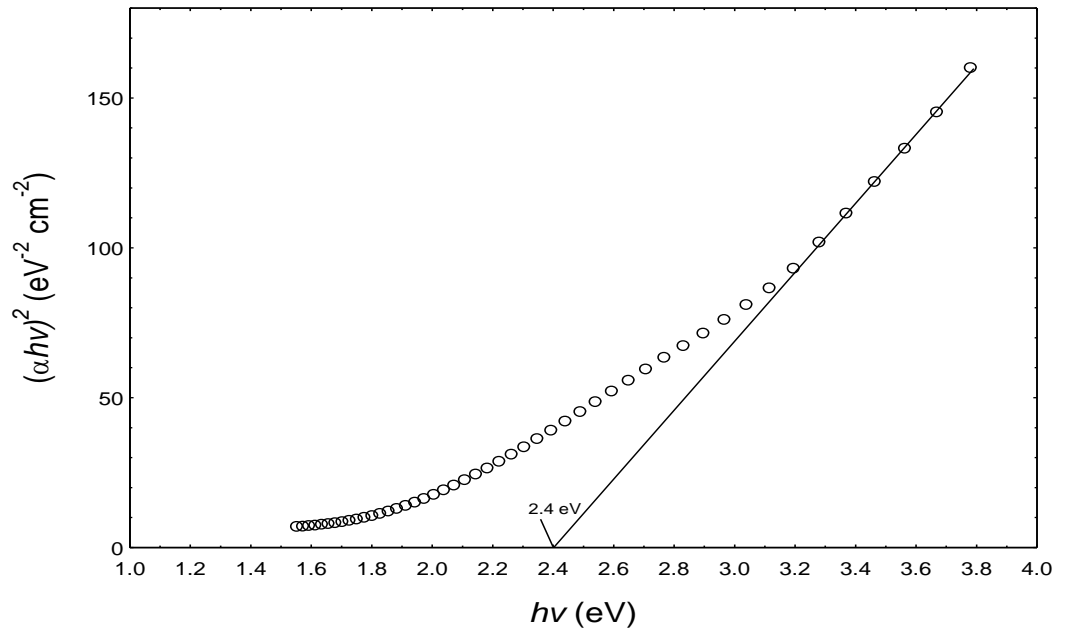
$$\alpha hv = A(hv - E_g)^n$$

Where A is the constant, E_g is the band gap, hv is the photon energy and n is the exponent which determine the type of the electronic transition causing absorption. The value taken for direct forbidden is $\frac{1}{2}$ (Ambade *et al.*, 2006). The relation between $(\alpha hv)^2$ against hv for the seven samples are shown in Figure 4.8 - 4.10, respectively. The value of absorption coefficient (α) is calculated from the relation

$$\alpha = \frac{A}{t \log e}$$

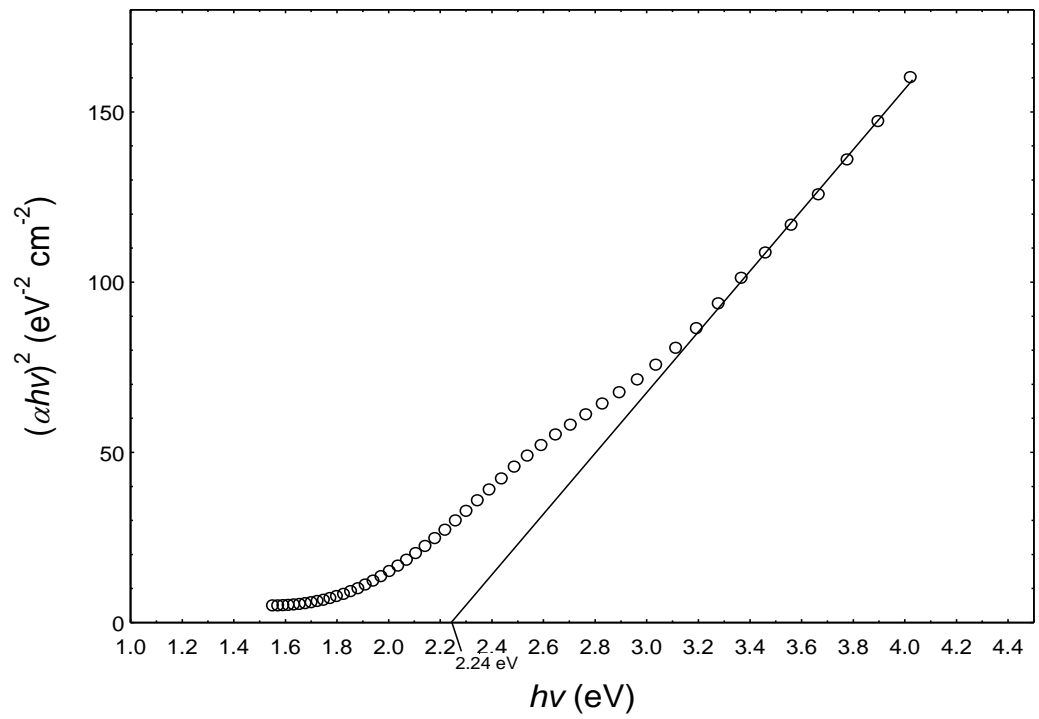
where A is absorption of the sample in UV and t is thickness of the cuvette.

S3020

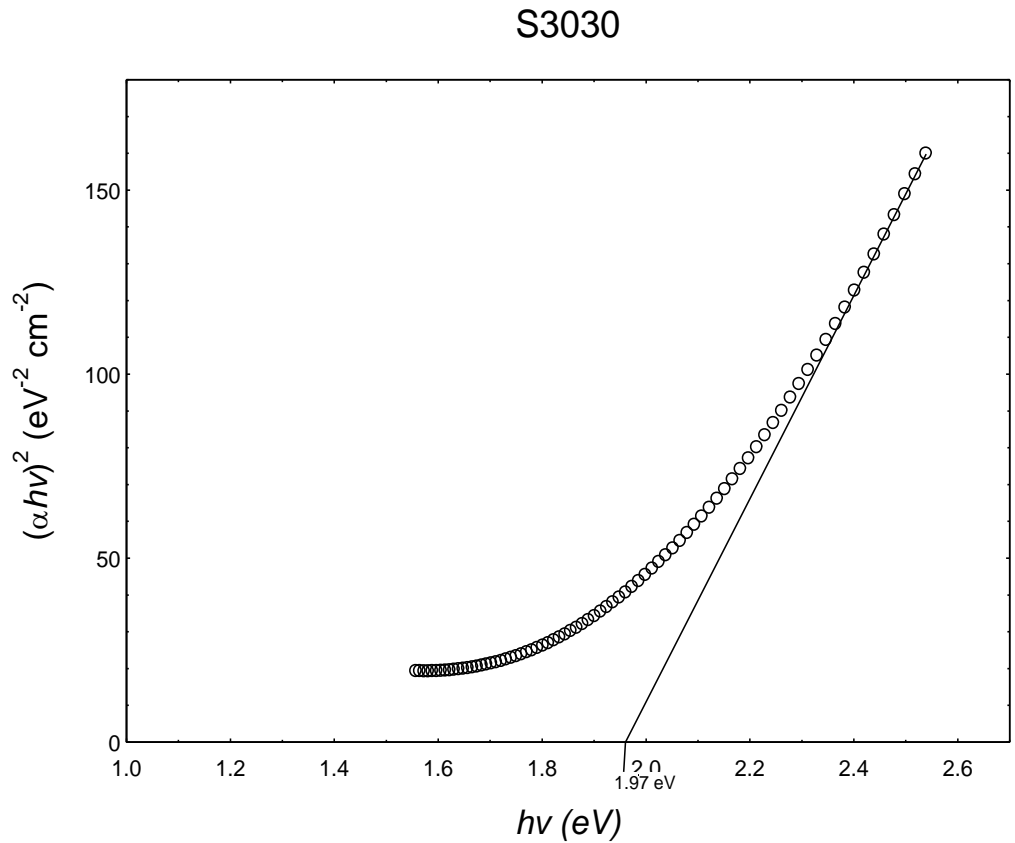


a.) Relation between $(\alpha h\nu)^2$ and photon energy ($h\nu$) for S3020

S3025

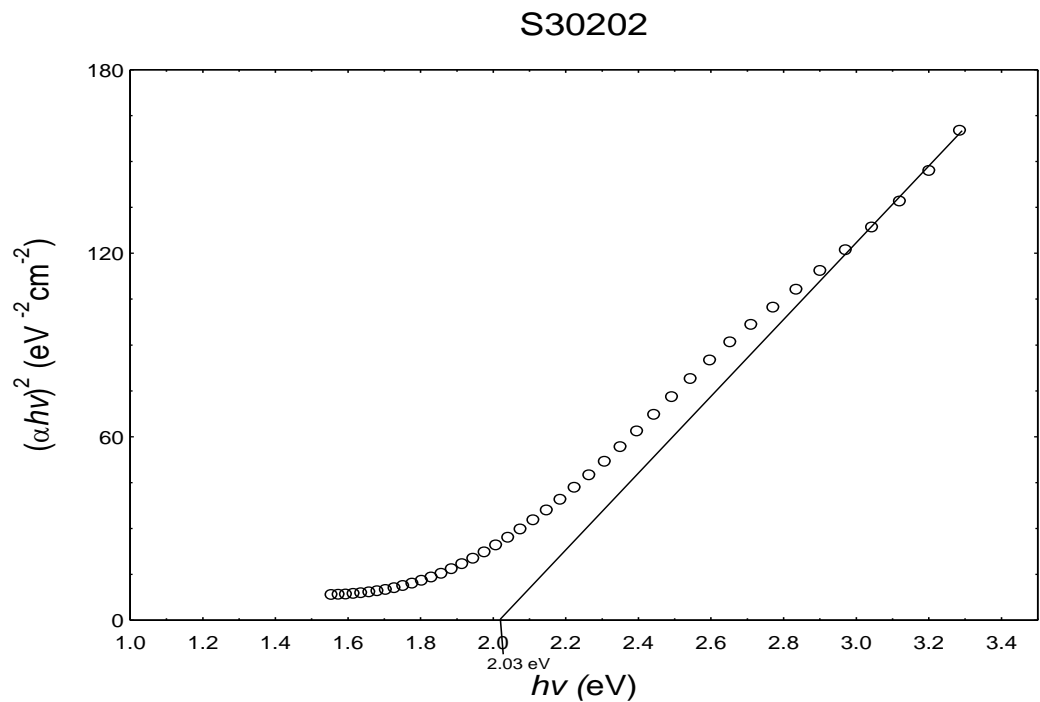


b.) Relation between $(\alpha h\nu)^2$ and photon energy ($h\nu$) for S3025

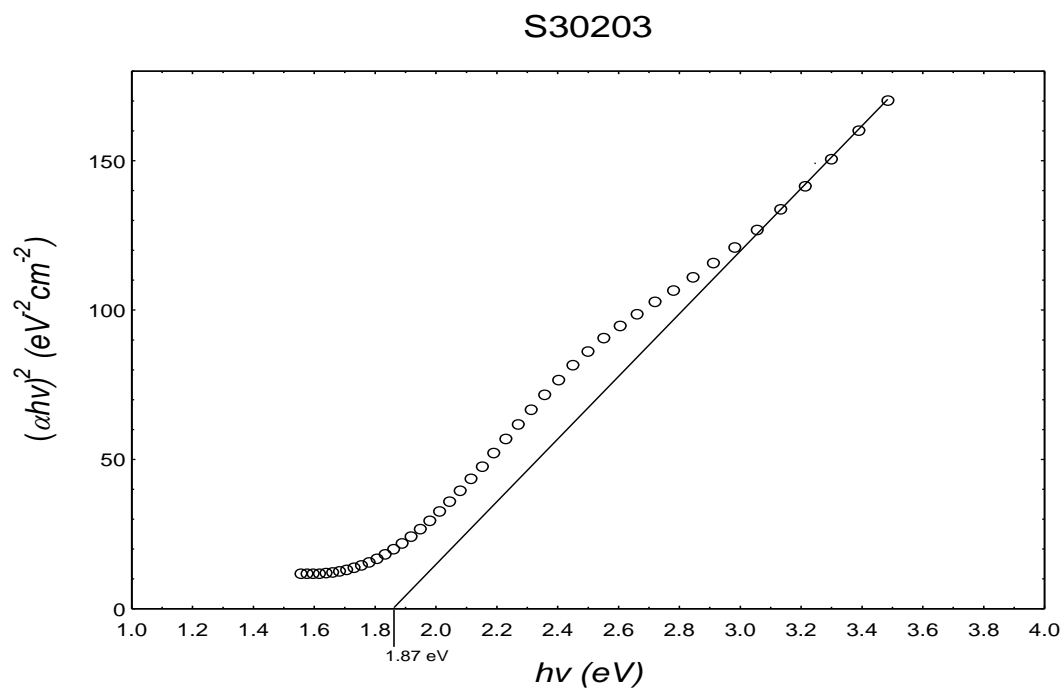


c.) Relation between $(\alpha hv)^2$ and photon energy ($h\nu$) for S3030

Figure 4.8: Relation between $(\alpha hv)^2$ and photon energy ($h\nu$) for CuSe nanoparticle prepared at various reducing agent, NaBH_4 . S3020 = 2.0 M, S3025 = 2.5 M and S3030 = 3.0 M

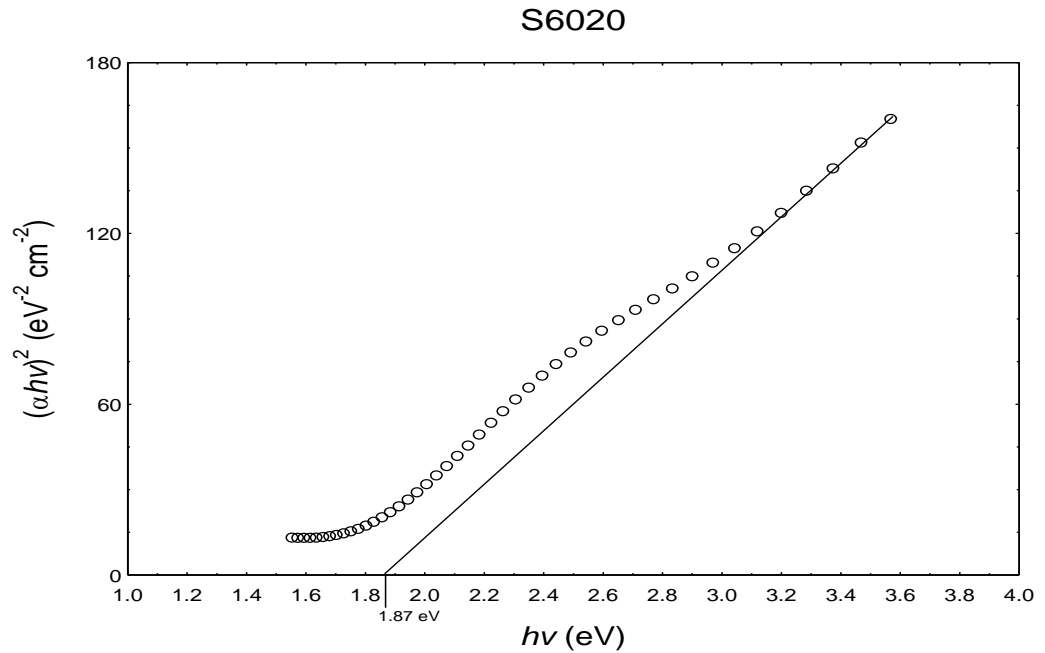


a.) Relation between $(\alpha hv)^2$ and photon energy ($h\nu$) for S30202

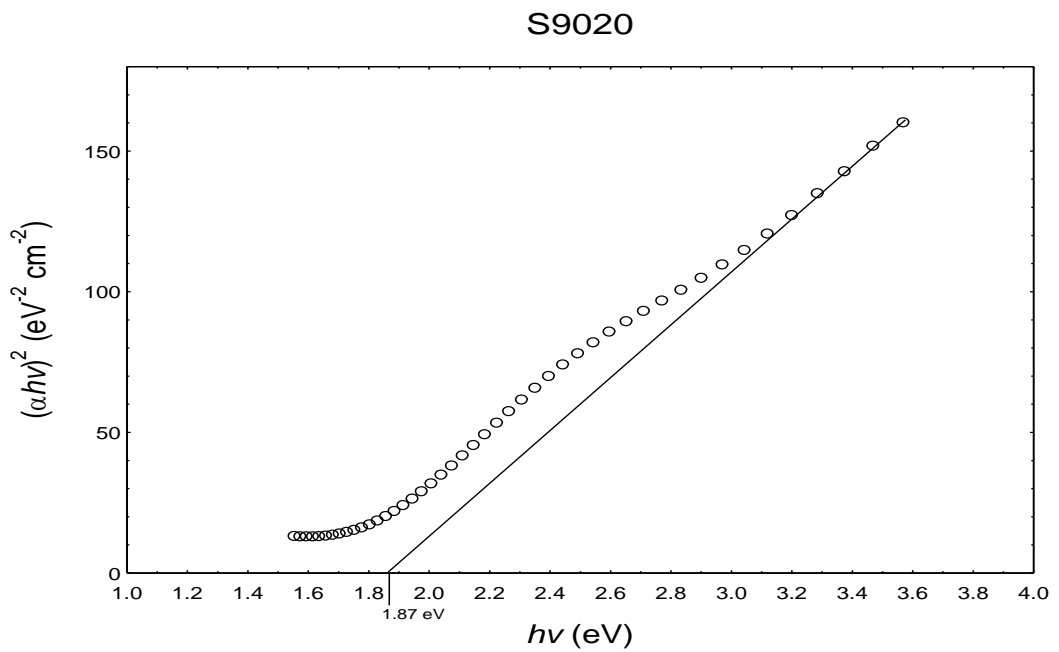


b.) Relation between $(\alpha hv)^2$ and photon energy ($h\nu$) for S30203

Figure 4.9: Relation between $(\alpha hv)^2$ and photon energy ($h\nu$) for CuSe nanoparticle prepared at various time of stirring. S3020 = 1 h, S30202 = 2 h and S30203 = 3h



a.) Relation between $(\alpha h\nu)^2$ and photon energy ($h\nu$) for S6020



b.) Relation between $(\alpha h\nu)^2$ and photon energy ($h\nu$) for S3020

Figure 4.10: Relation between $(\alpha h\nu)^2$ and photon energy ($h\nu$) for CuSe nanoparticle prepared at various time of stirring. S3020 = 30 mins, S6020 = 60mins and S9020 = 90 mins

From Figure 4.8 - 4.10, it can be observed that the optical band gap energy can be determined by extrapolating the curve to the energy axis for zero absorption coefficients. The optical band gap energies of CuSe nanoparticles have been estimated to be in the range of 1.87 – 2.40 eV which is direct band gap. The literature value for bulk CuSe is 1.30 eV (Seoudi, 2006). The comparison of the band gap value between samples values and literature band gap value are shown as below:

Table 4.5: Comparison of band gap energy values of samples prepared and literature band gap energy values.

Sample code	Band gap energy (eV)	Literature band gap energy (eV)
S3020	2.24	1.30
S3025	1.97	1.30
S3030	2.40	1.30
S6020	2.03	1.30
S9020	1.87	1.30
S30202	2.03	1.30
S30203	1.87	1.30

From the Table 4.5, it shows that optical band gap energy is inversely proportional to the crystallize size. Therefore, by increasing the concentration of reducing agent, stirring time and heated-treatment period will have effect on the band gap energy.

4.1.3 Photoluminescence (PL) Spectrophotometer

Figure 4.11 shows the control set that was run before the samples in order to ensure that the obtained emission peak did not originate from the solvent involved in the reaction. The control set (reference) is toluene.

The seven samples prepared at different parameters were characterised by photoluminescence spectrophotometer and the results achieved are shown in Figure 4.12 - 4.14, respectively.

Table 4.6: Summary of the emission peak and fluorescence intensity for all samples prepared in different parameters.

Samples code	Emission peak /nm	Fluorescence Intensity (FI)
S3020	438	572
S3025	438	575
S3030	438	575
S30202	438	572
S30203	438	572
S6020	438	574
S9020	438	574

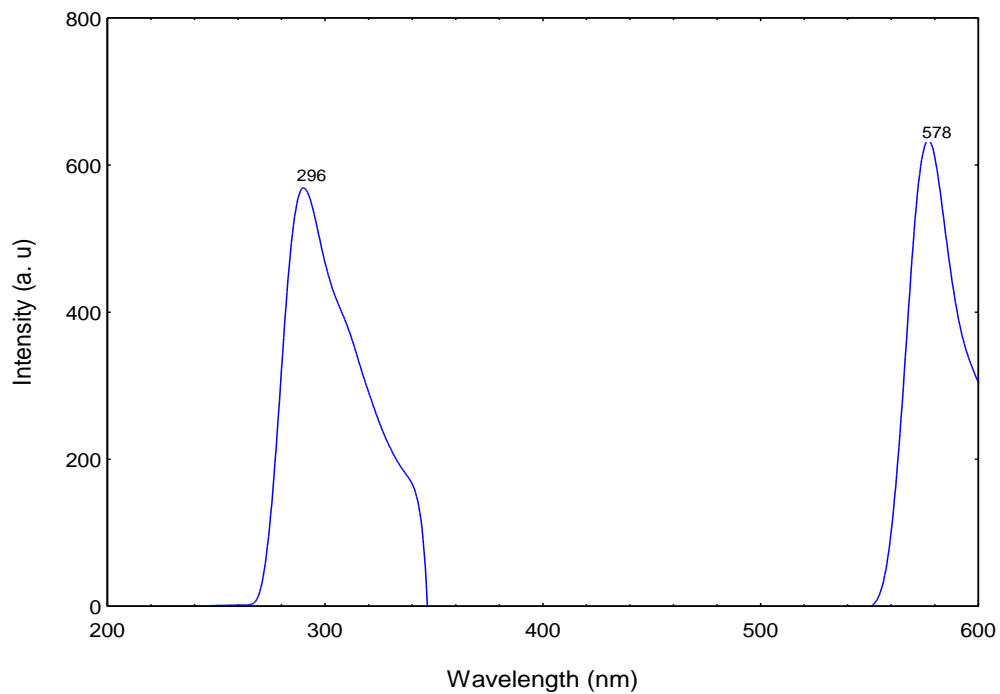


Figure 4.11: Photoluminescence spectrum of control set for the synthesis of copper selenide.

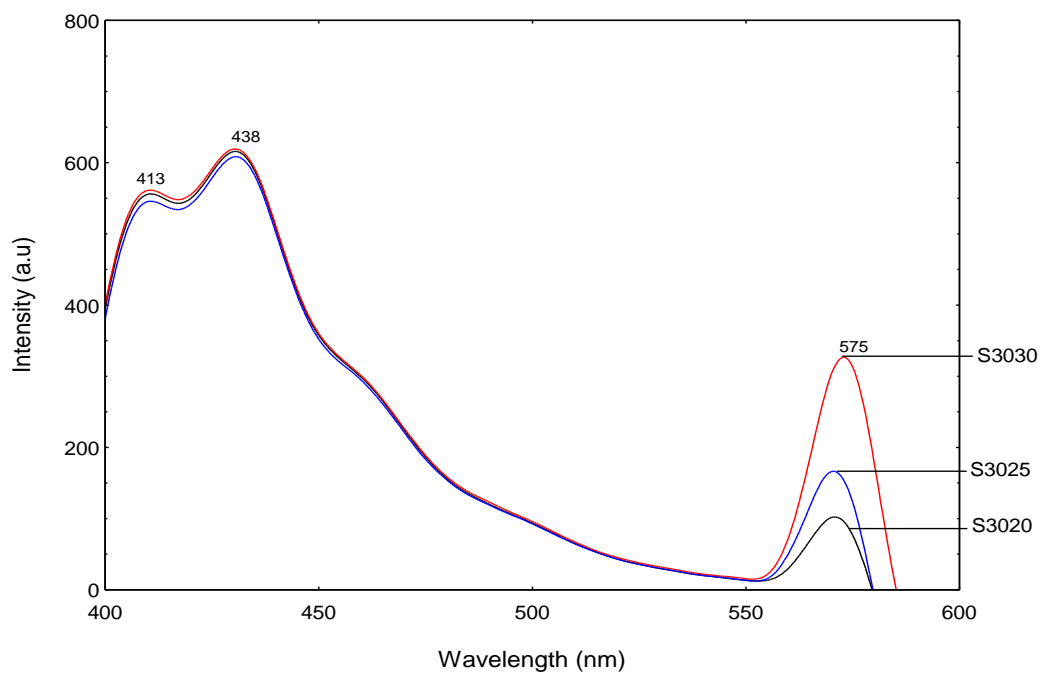


Figure 4.12: PL spectra of all the CuSe samples prepared at different concentration of reducing agent used.

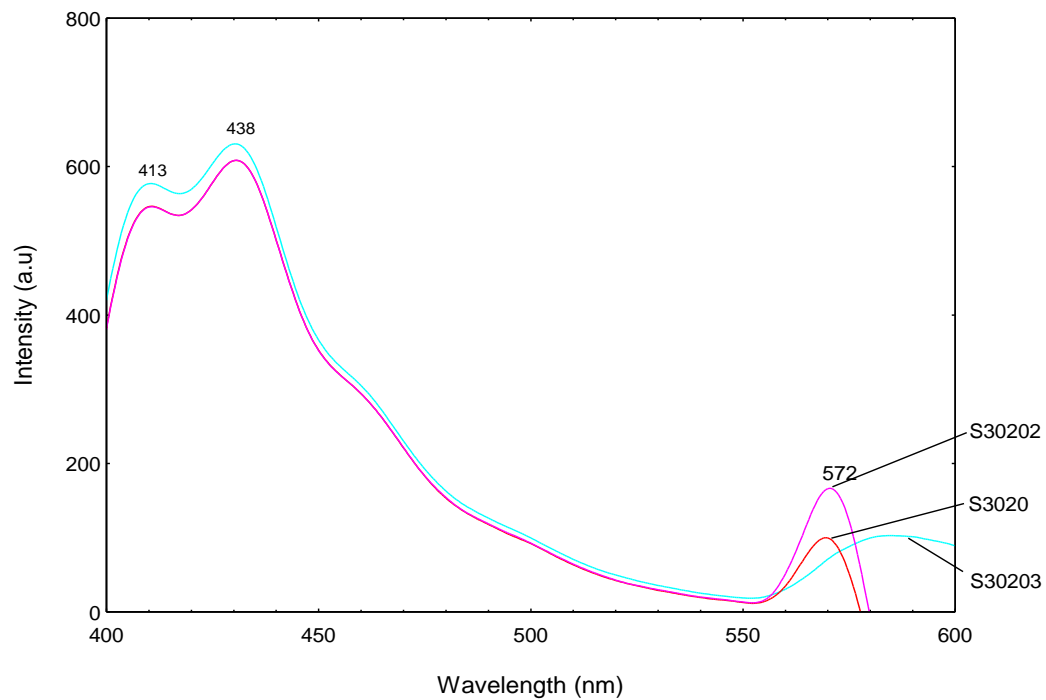


Figure 4.13: PL spectra of all the CuSe samples prepared at different stirring period.

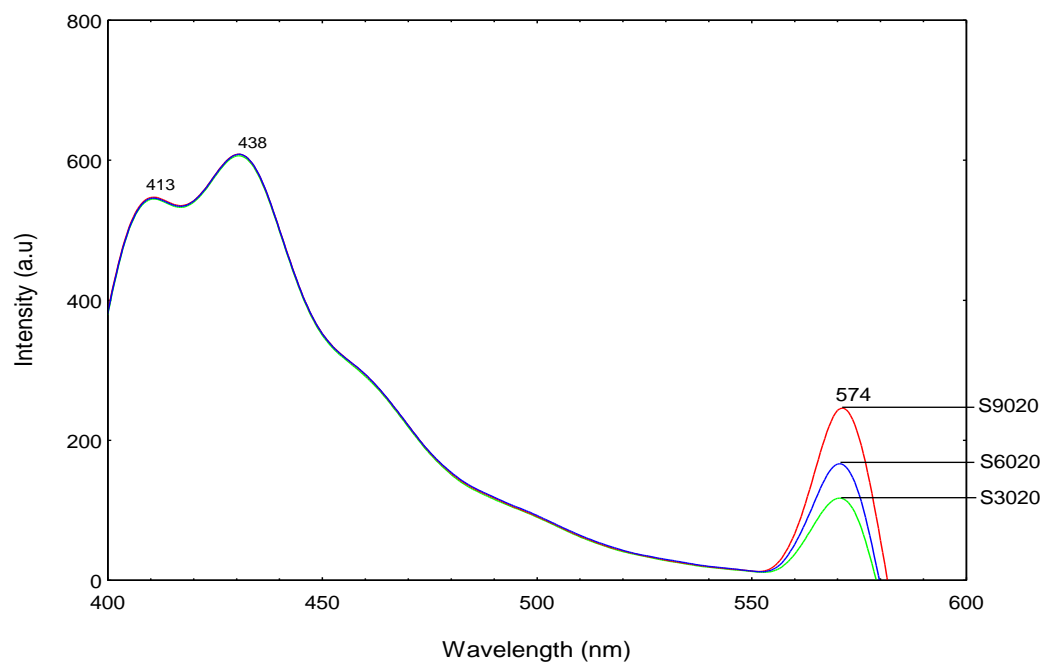


Figure 4.14: PL spectra of all the CuSe samples prepared at different heated-treatment period.

From the overlay absorption spectrum obtained throughout the Figure 4.12 - 4.14, all the seven samples showed an emission peak at around 438 nm. As compared to the control set spectrum (Figure 4.11), it can be seen that there is no significant emission peak at around 438 nm. The emission peak and fluorescence intensity for each sample is summarised in the Table 4.6. There is no obvious relationship between 3 parameters used and the emission peak of the sample.

All the seven samples showed a fluorescence emission peak at around 438 nm which belonged to the blue luminescence. The luminescence of copper can be brought about by exciting the sample with electrons, photons, or laser beams. With different synthetic method or surfactant employed, the emission peak positions can be distributed in the region of 320 – 520 nm. The photoluminescence property of copper selenide nanoparticles is depended on the size where its emission will shift to higher energy with decreasing the particles size. As the emission intensity and position is both dependant on the absorption of light source by the samples.

The fluorescence intensity of a sample is related to the quantum yield where the number of photons emitted is divided by the number of photons absorbed. Higher quantum yield would produce higher intensity and vice versa. In this experiment, the fluorescence intensities for all the seven samples are relatively high. The high quantum yield may be the reason of the visible

photoluminescence property was observed when the samples were examined under UV lamp. This may be due to the particles that are formed using this concentration is the most in particle quantity. As a result, more particles will absorb the light source and emit it as fluorescence.

CHAPTER 5

CONCLUSION

CuSe nanoparticles had been successfully synthesised using ternary oil in water (o/w) emulsion technique.

All of the samples were found to be existed in hexagonal phase. By increasing the concentration of reducing agent, stirring period and heated-treatment period, the mean crystallite size will be increased which varied between 1.87 – 2.40 nm. Due to this reason, the band gap energy was decreased. This is because the mean crystallite size is inversely proportional to the optical band gap energy of the compound. The optical band gap energies of CuSe nanoparticles in this research have been estimated to be in the range of 1.87 – 2.40 eV which is a direct band gap.

An emission peak was observed in the visible range at about 438 nm when the samples had been examined by Photoluminescence (PL) Spectrophotometer. PL peaks of CuSe were blue shift to the UV region due to the decrease in particles sizes led to increase band gap values correspondingly. The trend of the peaks decreased with increasing excitation wavelength also due to the PL were size-

dependent to the particles so more energy was needed in order to excite one electron from the valence band to conduction band.

In the future work, it is suggested using different of temperature, pressure, ageing time of emulsion, water to cyclohexane and reactants ratio, type of surfactant, and co-surfactant could be used in order to obtain different emulsion system. Therefore, the morphology of CuSe could be varied. Transmission electron microscopy (TEM) or scanning electron microscopy (SEM) should be carried out to check on the morphology and the size of the compound.

BIBLIOGRAPHY

Journal:

- Ago, H., Abe, H. and Shimizu, T. (2006). Experimental study on thermal characteristics of suspended platinum nanofilm sensors. *International Journal of Heat and Mass Transfer*, 49, 3879–3883
- Ambade, S. B., Mane, R. S., Kale, S. S., Sonawane, S. H., Tokle, T. and McClements D. J. (2010). Physicochemical properties of lactoferrin stabilized oil-in-water emulsions: Effects of pH, salt and heating. *Journal of Food Hydrocolloids*, 25, 976-982
- Asiyanbola, B. and Soboyejo, W. (2008). For the Surgeon: An Introduction to Nanotechnology. *Journal of Surgical Education*, 8, 137 - 144
- Bera, D., Qian, L., Tseng T. K. and Holloway, P. H. (2010). Quantum Dots and Their Multimodal Applications: A Review. *Materials*, 3, 2260-2345
- Bhattacharya, R. and Saha, S. (2008). Growth of CdS nanoparticles by chemical method and its characterization. *Journal of physics @ Indian Academy of Sciences*, 71, 187-192.
- Capek (2004). Preparation of metal nanoparticle in water-in-oil (w/o) microemulsion. *Journal of Advances in Colloid and Interface Science*, 110, 49-74.

- Gosavi, S. R., Deshpande, N. G., Gudagea, Y. G. and Sharma, R. (2007). Physical, optical and electrical properties of copper selenide (CuSe) thin films deposited by solution growth technique at room temperature. *Journal of Alloys and Compounds*, 448, 344–348
- Eastoe, J. Martin, J. H. and Maura H. (2006). Recent advances in Nanoparticle synthesis with reversed micelles. *Journal of colloid and interface science*, 259, 277-281
- Khiew P. S., Radiman, S., Huang, N. M. and Ahmad, M. S. (2003). Studies on the growth and characterisation of CdS and PbS nanoparticles using sugar-ester non-ionic water-in-oil microemulsion. *Journal of crystal Growth* 254, 235-243
- Kumar, P., Singh, K. and Srivastava O. N. (2010). Template free-solvothermally synthesised copper selenide (CuSe, Cu_{2-x}Se , $\beta\text{-Cu}_2\text{Se}$ & Cu_2Se) hexagonal nanoplates from different precursors at low temperature, *Journal of Crystal Growth*, 312, 2804–2813
- Kung, H. H. and Kung, M. C. (2004). Nanotechnology: applications and potentials for heterogeneous catalysis. *Journal of Catalysis Today*, 97 219–224
- Liu, J. C., Ikushima, Y. and Shervani Z. (2003). Environmentally benign preparation of metal nano-particles by using water-in- CO_2 microemulsions technology. *Journal of Current Opinion in Solid State and Materials Science*, 7, 255–261
- Lopez-Quintela, M. A. (2003). Synthesis of nanomaterials in microemulsions: formation mechanisms and growth control. *Current Opinion in Colloid and Interface Science*, 8, 137 - 144

- Lu, C. H., Lee, C. H. and Wu, C. H. (2010). Microemulsion-mediated solvothermal synthesis of copper indium diselenide powders. *Journal of Solar Energy Materials & Solar Cells*, 94, 1622–1626
- Mangalaraj, D., and Narayandass, S. K (2006). The effect of annealing on vacuum-evaporated copper selenide and indium telluride thin films. *Materials Characterization*, 58, 756–764
- Ohtsuki K.(2000). Evaluation of collision and stirring rates in circumplanetary particle disks based on three-body orbital integrations. *Current Opinion in Colloid and Interface Science*, 8, 128
- Peranantham, P., Jeyachandran, Y. L., Viswanathan, C., Praveena, N. N., Chitra, P. C., Hankare, P. P., Khomane, A. S., Chate, P. A., Rathod, K. C. and Garadkar, K. M. (2008). Preparation of copper selenide thin films by simple chemical route at low temperature and their characterization. *Journal of Alloys and Compounds*, 469, 478–482
- Sakr, G. B., Yahia, I. S., Fadel M., Fouad, S. S. and Romcevic N. (2010). Optical spectroscopy, optical conductivity, dielectric properties and new methods for determining the gap states of CuSe thin films. *Journal of Alloys and Compounds*, 507, 557–562
- Seoudi, R., Shabaka, A.A., Elokr, M.M., Seoudi, A. S. R., Shabaka, A. A. and Sobhi, A. (2006). Optical properties and electrical conductivity studies of copper selenide nanoparticle. *Journal of Materials Letters*, 61, 3451–3455
- Shaikh, A. V. and Han, S. H. (2006). Chemical synthesis of p-type nanocrystalline copper selenide thin films for heterojunction solar cells. *Journal of Applied Surface Science*, 253, 2123–2126

- Vinod, T. P., Jin, X. and Kim J. K. (2010). Hexagonal nanoplatelets of CuSe synthesized through facile solution phase reaction. *Materials Research Bulletin*, 46, 340 – 344
- Wang, C. C., Chen, A. L. and Chen, I. H. (2006). Effect of chelating functional polymer on the size of CdS nanocluster formation. *Journal of Colloid and Interface Science*, 293, 421–429
- Wei, W., Zhang, S. Y., Fang, C. X., Zhao S. Q., Jin, B. K., Zhang, X., Xie, H. Q., Fujii, M., Takahashi, K., Ikuta, T., Li, Y. Z., Gao X. D., Yang, C. and Huang F. Q. (2010). The effects of sputtering power on optical and electrical properties of copper selenide thin films deposited by magnetron sputtering. *Journal of Alloys and Compounds*, 505, 623–627
- Wu, J. and Tian, Y. (2007). Electrochemical behavior and electrogenerated chemiluminescence of crystalline CuSe nanotubes. *Journal of Solid State Sciences*, 10, 622-628
- Xu, J. and Li, Y. (2003). Formation of zinc sulfide nanorods and nanoparticles in ternary W/O microemulsion. *Journal of colloid and interface sciences*, 259, 275-281
- Zhang, X., Xie, H. Q., Fujii, M., Takahashi, K., Ikuta, T., Ago, H., Abe, H. and Shimizu, T. (2006). Experimental study on thermal characteristics of suspended platinum nanofilm sensors. *International Journal of Heat and Mass Transfer*, 49, 3879–3883
- Zainal, Z., Nagalingam, S. and Tan, C. L. (2005). Copper selenide thin films prepared using combination of chemical precipitation and dip coating method. *Materials Letter*, 59, 1391 - 1394

Books:

Atkins, P. and Paula, J. D. (2006). Atkins' Physical Chemistry. 8th Edition. (pp 690 – 728). New York: Oxford.

Dann, S. (2002). Reaction and Characterization of Solids. 1st Edition. p. 55-57. New York: John Wiley & Sons, Inc.

Dutta, P. and Gupta, S. (2008). Understanding of Nano Science and technology, 1st Edition. p. 1-2. New Delhi: Global Vision Publishing House.

Hammond, C. (2009). The basics of crystallography and diffraction 3rd Edition. (pg 196-198). New York: Oxford University Press Inc.

Housecroft, C. E. and Sharpe, A. G. (2008). Inorganic Chemistry. 3rd Edition. P. 167. Pearson Education, Inc.

Ian D. M. and Ross, S. (2002). Colloidal Dispersions Suspensions, Emulsions, and Foams. Wiley-Interscience: John Wiley & Sons, Ltd.

Kelsall, Robert W., Hamley, Ian W., and Geoghegan, M. (2005). Nanotechnology: Nanoscale science and technology. (pp 1-5, 131-135, 259). West Sussex: John Wiley & Sons, Ltd.

Manasi K. (2008). Nanotechnology: Fundamental and Application (pp 14, 51-58). New Dehli: I.K International Publishing House Pvt. Ltd.

Pradeep, T (2008). Nano: The Essentials understanding anoscience and nanotechnology. (pp 75-81, 123-125, 186-196, 307-309). 7 West Patel Nagar, New Delhi: Tata McGraw-Hill Publisher.

Ratner, M. and Ratner, D. (2003). Nanotechnology: A gentle Introduction to The Next big Idea (pp 6-7). Pearson Education, Inc.

Rouessac, F. and Rouessac, A. (1994). Chemical Analysis: Modern Instrumentation Methods and Techniques (pp 167-173) John Wiley & Sons, Ltd.

Silberberg, M. S. (2009). Chemistry The Molecular nature of Matter and Change. 5th Edition. (pp 489 – 491). New York:McCraw-Hill companies, Inc.

Smart, L. and Moore, E. (2005). Solid State Chemistry: An Introduction. 3rd Edition. (pp 27, 77-82, 89). United States: Taylor & Francis Group, LLC.

Websites:

A schematic diagram of a powder diffractometer. URL:
http://chemwiki.ucdavis.edu/analytical_chemistry/instrumental_analysis/powder_x-ray_diffraction. Accessed on 6st November 2010.

Colloidal quantum dots irradiated with a UV light. Different sized quantum dots emit different color light due to quantum confinement. URL:
<http://www.mdpi.com/1996-1944/3/4/2260/pdf>. Accessed on 1 July 2010.

Applications of Nanotechnology. URL:
http://www.nanowerk.com/nanotechnology/introduction/introduction_to_nanotechnology_12.php

Comparison of emulsion and microemulsion. URL:
<http://www.pharmainfo.net/reviews/microemulsions-novel-drug-delivery-vehicle>. Accessed on 7 July 2010.

CuSe and Its application. Retrieved from Principles of Semiconductor Devices
URL:
http://www.nanowerk.com/nanotechnology/introduction/introduction_to_nanotechnology_7.php. Accessed on 6 July 2010.

Diagram of double beam UV/Vis spectrometer. URL:

http://www.chemistry.mtu.edu/~hyliu/ch4212/Powerpoint/An_introduction_%20to_ultraviolet_Visible.pdf. Accessed on 23 July 2010.

E-k diagram illustrating

- a) Photon absorption in a direct band gap semiconductor
- b) Photon absorption in an indirect band gap semiconductor assisted by phonon absorption and
- c) Photon absorption in an indirect band gap semiconductor assisted by phonon emission. URL:

http://ecee.colorado.edu/~bart/book/book/chapter4/ch4_6.htm. Accessed on 23 December 2010.

Energy level diagram of fluorescence occurrence. URL:

<http://web.njit.edu/~gary/321/Lecture5.html>. Accessed on 23 July 2010.

Nanomaterial. URL: <http://www.scribd.com/doc/13787393/Nano-Materials>.

Accessed on 23 July 2010.

Nanotechnology: The New Era of Science. URL:

<http://www.docstoc.com/docs/39210887/Nanotechnology-The-New-Era-of-Science-F>. Accessed on 27 August 2010.

Molecular structures of a single-walled carbon nanotube (SWNT) and of a multi-walled carbon nanotube (MWNT). URL:

http://www-ibmc.ustrasbg.fr/ict/vectorisation/nanotubes_eng.shtml. Accessed on 27 August 2010.

Schematic representation of the building up of Nanostructures. URL:

http://www.gitam.edu/eresource/nano/nanotechnology/role_of_bottomup_and_topdown_a.htm. Accessed on 1st November 2010.

The band diagram for nano-sized crystals of semiconductor (quantum dots). URL:

<http://www3.imperial.ac.uk/>. Accessed on 23 December 2010.

The comparison of size with different matters. URL:

<http://nanoscience.massey.ac.nz/>. Accessed on 2 July 2010.

APPENDICES

APPENDIX A

Example Calculation for the mole and mass of CTAB,

$$\begin{aligned} \text{Mole} &= \frac{(\text{Molarity} \times \text{Volume})}{1000} \\ &= \frac{(0.1 \text{ mol dm}^{-3} \times 10 \text{ mL})}{1000} \\ &= 0.001 \text{ mol} \end{aligned}$$

$$\begin{aligned} \text{Mass} &= \text{mole} \times \text{Molecular weight of CTAB} \\ &= 0.001 \text{ mol} \times 364.48 \text{ gmol}^{-1} \\ &= 0.3645 \text{ g} \end{aligned}$$

Example Calculation for the mole and mass of $\text{CuCl}_2 \cdot 2\text{H}_2\text{O}$,

$$\begin{aligned} \text{Mole} &= \frac{(\text{Molarity} \times \text{Volume})}{1000} \\ &= \frac{(0.1 \text{ mol dm}^{-3} \times 50 \text{ mL})}{1000} \\ &= 0.005 \text{ mol} \end{aligned}$$

$$\begin{aligned} \text{Mass} &= \text{mole} \times \text{Molecular weight of } \text{CuCl}_2 \cdot 2\text{H}_2\text{O} \\ &= 0.005 \text{ mol} \times 170.48 \text{ gmol}^{-1} \\ &= 0.8524 \text{ g} \end{aligned}$$

Example Calculation for the mole and mass of Na_2SeO_3 ,

$$\begin{aligned} \text{Mole} &= \frac{(\text{Molarity} \times \text{Volume})}{1000} \\ &= \frac{(0.1 \text{ mol dm}^{-3} \times 50 \text{ mL})}{1000} \\ &= 0.005 \text{ mol} \end{aligned}$$

$$\begin{aligned} \text{Mass} &= \text{mole} \times \text{Molecular weight of } \text{Na}_2\text{SeO}_3 \\ &= 0.005 \text{ mol} \times 172.96 \text{ gmol}^{-1} \\ &= 0.8648 \text{ g} \end{aligned}$$

Example Calculation for the mole and mass of NaBH_4 ,

$$\begin{aligned} \text{Mole} &= \frac{(\text{Molarity} \times \text{Volume})}{1000} \\ &= \frac{(2.0 \text{ mol dm}^{-3} \times 5 \text{ mL})}{1000} \\ &= 0.01 \text{ mol} \end{aligned}$$

$$\begin{aligned} \text{Mass} &= \text{mole} \times \text{Molecular weight of } \text{NaBH}_4 \\ &= 0.01 \text{ mol} \times 37.83 \text{ gmol}^{-1} \\ &= 0.3783 \text{ g} \end{aligned}$$

Note: The mole and concentration of the CTAB, $\text{CuCl}_2 \cdot 2\text{H}_2\text{O}$, NaSe_2O_3 and NaBH_4 used were calculated for each parameters and tabulated as below:-

Preparation of samples at various concentration of reducing agent (NaBH₄)

Sample	DI H ₂ O (mL)	Cyclohexane (mL)	CTAB		Cu ²⁺			Se ²⁻			Time of stirring	Autoclave	Conc. of NaBH ₄ (mol dm ⁻³)
			Conc. (mol dm ⁻³)	Mole	Conc. (mol dm ⁻³)	Vol. of DI to dissolve (mL)	Mole	Conc. (mol dm ⁻³)	Vol. of DI to dissolve (mL)	Mole			
S3020	10	5	0.1	0.001	0.1	50	0.005	0.1	50	0.005	1h	30 mins, 121 ^o c	2.0
S3025	10	5	0.1	0.001	0.1	50	0.005	0.1	50	0.005	1h	60 mins, 121 ^o c	2.5
S3030	10	5	0.1	0.001	0.1	50	0.005	0.1	50	0.005	1h	90 mins, 121 ^o c	3.0

Preparation of samples at different time of stirring

Sample	DI H ₂ O (mL)	Cyclohexane (mL)	CTAB		Cu ²⁺			Se ²⁻			Time of stirring	Autoclave	Conc. of NaBH ₄ (mol dm ⁻³)
			Conc. (mol dm ⁻³)	Mole	Conc. (mol dm ⁻³)	Vol. of DI to dissolve (mL)	Mole	Conc. (mol dm ⁻³)	Vol. of DI to dissolve (mL)	Mole			
S3020	10	5	0.1	0.001	0.1	50	0.005	0.1	50	0.005	1h	30 mins, 121 ^o c	2.0
S30202	10	5	0.1	0.001	0.1	50	0.005	0.1	50	0.005	2h	30 mins, 121 ^o c	2.0
S30203	10	5	0.1	0.001	0.1	50	0.005	0.1	50	0.005	3h	30 mins, 121 ^o c	2.0

Preparation of samples at different heated-treatment period

Sample	DI H ₂ O (mL)	Cyclohexane (mL)	CTAB		Cu ²⁺			Se ²⁻			Time of stirring	Autoclave	Conc. of NaBH ₄ (mol dm ⁻³)
			Conc. (mol dm ⁻³)	Mole	Conc. (mol dm ⁻³)	Vol. of DI to dissolve (mL)	Mole	Conc. (mol dm ⁻³)	Vol. of DI to dissolve (mL)	Mole			
S3020	10	5	0.1	0.001	0.1	50	0.005	0.1	50	0.005	1h	30 mins, 121 ^o c	2.0
S6020	10	5	0.1	0.001	0.1	50	0.005	0.1	50	0.005	1h	60 mins, 121 ^o c	2.0
S9020	10	5	0.1	0.001	0.1	50	0.005	0.1	50	0.005	1h	90 mins, 121 ^o c	2.0

APPENDIX B

The calculated β values and mean crystallite sizes for the selected samples S3020, S3025 and S3030.

Sample code	FWHM in 2θ ($^\circ$)	β calculated from FWHM in radian	2θ of (110) peak ($^\circ$)	θ of (110) peak ($^\circ$)	Calculated mean crystallite size (nm)
S3020	1.0709	0.0187	45.4245	22.7123	8.0447
S3025	0.9943	0.0174	45.2582	22.6291	8.6405
S3030	0.4236	0.0074	44.9708	22.4854	20.2958

<p>The formula for calculations of β,</p> $\beta = \frac{FWHM \text{ in } 2\theta \times \pi}{180^\circ}$	<p>The formula for calculations of D,</p> $D = \frac{K \lambda}{\beta \cos \theta}$
<p>For sample S3020,</p> $\beta = \frac{1.0709 \times \pi}{180^\circ}$ $= 0.0187$	<p>For sample S3020,</p> $D = \frac{0.9 \times 1.5419 \text{ \AA}}{0.0187 \cos (22.7123)}$ $= 8.0447 \text{ nm}$
<p>For sample S3025,</p> $\beta = \frac{0.9943 \times \pi}{180^\circ}$ $= 0.0174$	<p>For sample S3025,</p> $D = \frac{0.9 \times 1.5419 \text{ \AA}}{0.0174 \cos (22.6291)}$ $= 8.6405 \text{ nm}$
<p>For sample S3030,</p> $\beta = \frac{0.4236 \times \pi}{180^\circ}$ $= 0.0074$	<p>For sample S3030,</p> $D = \frac{0.9 \times 1.5419 \text{ \AA}}{0.0074 \cos (22.4854)}$ $= 20.2958 \text{ nm}$

The calculated β values and mean crystallite sizes for the selected samples S3020, S30202 and S30203.

Sample code	FWHM in 2θ ($^\circ$)	β calculated from FWHM in radian	2θ of (110) peak ($^\circ$)	θ of (110) peak ($^\circ$)	Calculated mean crystallite size (nm)
S3020	1.0709	0.0187	45.4245	22.7123	8.0447
S30202	0.8022	0.0140	45.2800	22.6400	10.7398
S30203	0.5580	0.0097	45.2033	22.6017	15.4964

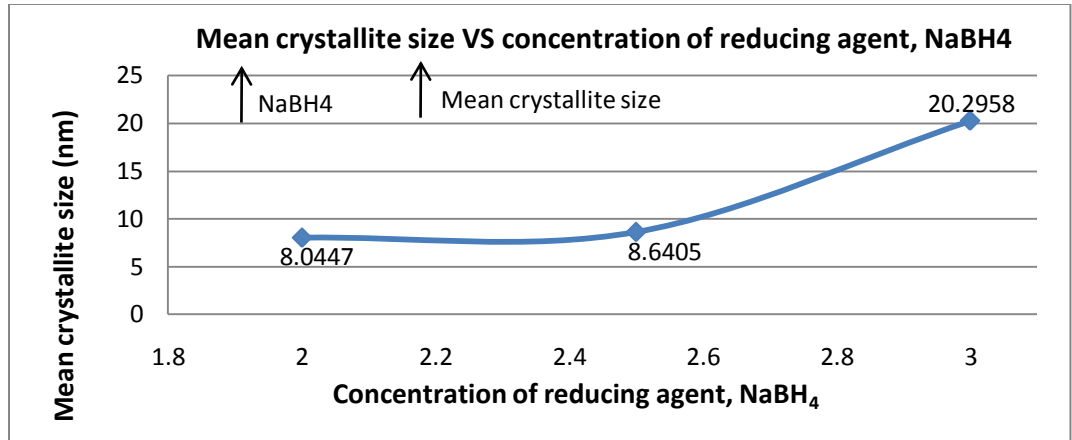
<p>The formula for calculations of β,</p> $\beta = \frac{FWHM \text{ in } 2\theta \times \pi}{180^\circ}$	<p>The formula for calculations of D,</p> $D = \frac{K \lambda}{\beta \cos\theta}$
<p>For sample S3020,</p> $\beta = \frac{1.0709 \times \pi}{180^\circ}$ <p>= 0.0187</p>	<p>For sample S3020,</p> $D = \frac{0.9 \times 1.5419 \text{ \AA}}{0.0187 \cos(22.7123)}$ <p>= 8.0447 nm</p>
<p>For sample S6020,</p> $\beta = \frac{0.8022 \times \pi}{180^\circ}$ <p>= 0.0140</p>	<p>For sample S6020</p> $D = \frac{0.9 \times 1.5419 \text{ \AA}}{0.014 \cos(22.6400)}$ <p>= 10.7398 nm</p>
<p>For sample S9020,</p> $\beta = \frac{0.5580 \times \pi}{180^\circ}$ <p>= 0.0097</p>	<p>For sample S9020</p> $D = \frac{0.9 \times 1.5419 \text{ \AA}}{0.0097 \cos(22.6017)}$ <p>= 15.4964 nm</p>

The calculated β values and mean crystallite sizes for the selected samples S3020, S6020 and S9020.

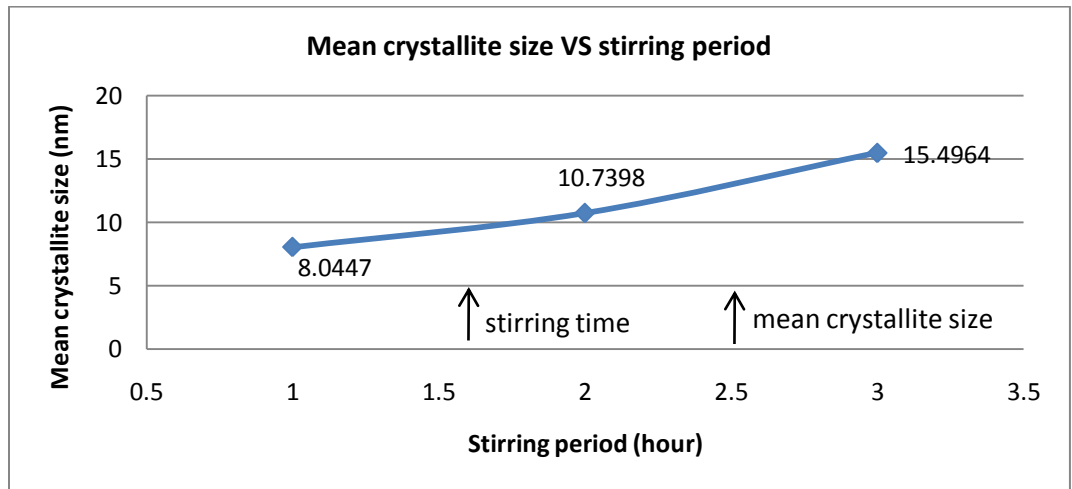
Sample code	FWHM in 2θ ($^{\circ}$)	B calculated from FWHM in radian	2θ of (110) peak ($^{\circ}$)	θ of (110) peak ($^{\circ}$)	Calculated mean crystallite size (nm)
S3020	1.0709	0.0187	45.4245	22.7123	8.0447
S6020	0.8855	0.0155	45.2062	22.6031	9.6979
S9020	0.6247	0.0109	45.3018	22.6509	13.7953

<p>The formula for calculations of β,</p> $\beta = \frac{FWHM \text{ in } 2\theta \times \pi}{180^{\circ}}$	<p>The formula for calculations of D,</p> $D = \frac{K \lambda}{\beta \cos \theta}$
<p>For sample S3020,</p> $\beta = \frac{1.0709 \times \pi}{180^{\circ}}$ $= 0.0187$	<p>For sample S3020,</p> $D = \frac{0.9 \times 1.5419 \text{ \AA}}{0.0187 \cos (22.7123)}$ $= 8.0447 \text{ nm}$
<p>For sample S6020,</p> $\beta = \frac{0.8855 \times \pi}{180^{\circ}}$ $= 0.0155$	<p>For sample S6020,</p> $D = \frac{0.9 \times 1.5419 \text{ \AA}}{0.0155 \cos (22.6031)}$ $= 9.6979 \text{ nm}$
<p>For sample S9020,</p> $\beta = \frac{0.6247 \times \pi}{180^{\circ}}$ $= 0.0109$	<p>For sample S9020,</p> $D = \frac{0.9 \times 1.5419 \text{ \AA}}{0.0109 \cos (22.6509)}$ $= 13.7953 \text{ nm}$

Graph of mean crystallite size Vs concentration of reducing agent



Graph of mean crystallite size Vs stirring period



Graph of mean crystallite size Vs heated-treatment period

